Institut für Veterinärpathologie
der Vetsuisse-Fakultät Universität Zürich

Direktorin Institut: Prof. Dr. med. vet Anja Kipar

Arbeit unter wissenschaftlicher Betreuung von
Prof. Dr. med. vet Anja Kipar

Morphological and immunophenotypic features of human CD34+ hematopoietic stem cell-engrafted NSG mice

Inaugural-Dissertation

zur Erlangung der Doktorwürde der
Vetsuisse-Fakultät Universität Zürich

vorgelegt von

Sandra Larissa Elena Blümich

Tierärztin
aus Berlin, Deutschland

genehmigt auf Antrag von

Prof. Dr. med. vet Anja Kipar, Referentin
Prof. Dr. rer. nat. Thorsten Buch, Korreferent

2020

Index

Vetsuisse Faculty University of Zurich (2020)

Sandra Larissa Elena Blümich

Institute of Veterinary Pathology

ivpz@vetpath.uzh.ch

Morphological and immunophenotypic features of human CD34+ hematopoietic stem cell-engrafted NSG mice

Immunodeficient mice engrafted with human immune system cells are animal models for the study of human diseases. Immunophenotyping of these mice mostly focuses on engraftment rates and cellular differentiation in blood and secondary lymphoid organs and is performed by FACS analysis; there is limited information on the morphological aspects of the engraftment and the prevalence of histopathological lesions.

We histologically examined young NSG mice, naïve and engrafted with $CD34^+$ human hemopoietic stem cells (HSC), undertook quantitative immunohistochemical analyses and compared the results with those of FACS analyses.

Besides well-known incidental organ findings, NSG mice only exhibited a case of lymphoblastic lymphoma in a 6-month-old animal, whereas in mice engrafted with human HSC nephropathy, ovarian atrophy, cataract and abnormal retinal development secondary to irradiation were frequent. The latter also often exhibited multisystemic granulomatous inflammatory infiltrates, interpreted as graft versus host disease. They had variable repopulation rates in hemolymphatic organs, which did not always parallel the engraftment levels measured via FACS.

The study provides a catalogue of the most common pathological features to consider in young NSG mice without and after human HSC engraftment. This and the knowledge on the relevant features of engraftment at tissue level will assist in the morphological assessment of this animal model in experimental settings.

Keywords: NSG mice, $CD34^+$ stem cell engraftment, humanized mouse, phenotyping, graft versus host disease, lymphoma

Vetsuisse-Fakultät Universität Zürich (2020)

Sandra Larissa Elena Blümich

Institut für Veterinärpathologie

ivpz@vetpath.uzh.ch

Morphologische und immunphänotypische Eigenschaften von CD34+ stammzelltransplantierten NSG Mäusen

Mit humanen Immunzellen transplantierte immundefiziente Mäuse dienen als Modelle zur Untersuchung menschlicher Krankheiten. Ihre Immunphänotypisierung erfolgt durch Quantifizierung der Transplantationsrate und der zellulären Differenzierung in Blut und lymphatischen Organen mittels FACS-Analyse. Bisher liegen kaum Informationen zu pathologischen Folgen und morphologischen Aspekten der Transplantation vor.
Junge, naive oder mit $CD34^+$ humanen Stammzellen transplantierte NSG-Mäuse wurden histologisch und quantitativ immunhistologisch untersucht. Letztere dienten zum Vergleich mit parallel durchgeführten FACS-Analysen.
Neben bekannten Zufallsbefunden an Organen fand sich bei den naiven NSG-Mäusen lediglich ein Fall eines lymphoblastischen Lymphoms bei einem 6 Monate alten Tier, bei transplantierten Mäusen dagegen häufig eine strahlenbedingte Nephropathie, Ovaratrophie, Katarakt und abnormale Entwicklung der Retina. Letztere Tiere wiesen oft multisystemische granulomatöse Entzündungsherde auf, die als Graft versus Host Disease interpretiert wurden. Die Repopulationsraten im hämolymphatischen Gewebe waren variabel und korrelierten nicht immer mit den FACS-Ergebnissen.
Die Studie liefert einen Katalog der häufigsten pathologischen Veränderungen bei jungen NSG-Mäusen ohne und nach humaner Stammzelltransplantation. Dieser kann, ebenso wie das neu gewonnene Wissen zum Effekt der Transplantation im Gewebe, für morphologische Untersuchungen unter experimentellen Bedingungen hilfreich sein.

Stichwörter: NSG Mäuse, $CD34^+$ Stammzellentransplantation, humanisierte Mäuse, Phänotypisierung, Graft versus Host Disease, Lymphom

Morphological and immunophenotypic features of human CD34$^+$ hematopoietic stem cell-engrafted NSG mice

Introduction

Recent advances in the generation of humanized murine models, featuring immunodeficient mice engrafted with human immune system cells, have brought tangible breakthroughs in numerous research fields, such as the preclinical development of immunotherapeutic agents and the study of infectious, metabolic and autoimmune diseases. Progress has been facilitated by the optimisation of immunodeficient mouse models, which, being deprived of acquired and innate immunity, can be transplanted with human cells that eventually develop into a variably functional immune system in the model.[9,40,49,53]

Among the numerous immunodeficient mouse strains available, the NOD-scid IL-2Rγ^{null} (NSG) mouse represents the currently most widely used option for successful humanisation of the immune system, showing one of the highest engraftment rates among the various strains.[27,55] NSG mice are non-obese diabetic (NOD) mice bearing the Prkdc^{scid} mutation and a genetic deletion of the common γ chain of the IL-2 receptor. Accordingly, they exhibit defects in the lymphoid cell development, lacking both innate and adaptive lymphocytes, and have diminished complement activity due to C5 deficiency.[9,23,44] In contrast to their NOD/scid predecessors, NSG mice are not prone to develop thymic lymphomas; they have a long life span of about two years.[9,22] Functional immune system abnormalities in immunodeficient mice are associated with abnormal development of the primary and secondary lymphoid organs; however, the morphological equivalents of the latter vary across the available models.[42] NSG mice, for example, exhibit a small spleen, thymus and lymph nodes that lack lymphoid structures and are composed almost exclusively of reticular stromal cells.[41,43,44]

Immunodeficient mice can be transiently or stably humanized by administration of human mature lymphoid or CD34$^+$ hematopoietic stem cells (HSC), respectively.[53] Most models allow multi-lineage human immune cell engraftment and both the acquired and innate human immune system components develop at variable quantities. The present study focuses on CD34$^+$ HSC humanized NSG (hu-NSG) mice, a model in which T and B cell engraftment is generally successful, though without consistent immunoglobulin (Ig) class switching and only IgM production by B cells.[18,40,48] Hu-NSG mice exhibit human dendritic cells, NK cells and myeloid cells including neutrophils.[24,31,52] However, the latter two are generally seen at low numbers, and seem to be defective in their maturation and function.[18,22,40,49] It has been shown that the reconstituted human leukocytes form variably sized aggregates in the lymphoid organs of these mice, which in general do not form distinctive secondary lymphoid structures such as lymphoid follicles in spleen and lymph nodes.[22,49,52] In the thymus, repopulation appears to be more efficient in immunodeficient mice transplanted shortly after birth, whilst in mice engrafted at adult age the thymus is less prone to support human cell engraftment.[7,54] In the bone marrow the proportion of lymphoid and myeloid cells varies, as different published studies indicate.[52,54]

Effective engraftment in hu-NSG mice is generally determined by fluorescent activated cell sorting (FACS) analysis of the blood, usually at 12-16 weeks post-engraftment. The FACS data suggest that depending on the age of the mice, the source and manipulation of the HSC as well as the administration route, the extent of

engraftment can vary substantially.[22,25] So far, most of the immunophenotyping data that is available for these mice are also based on FACS analyses, carried out on circulating and organ-specific immune cells at different endpoints.[7,25,35,48] Accordingly, there is very limited information concerning the *in situ* aspects of engraftment, in particular in the hemolymphatic tissues and, specifically, how these correlate with the engraftment rates and cellular differentiation determined by FACS. Furthermore, little is known about the incidence of spontaneous diseases and common histopathological lesions in hu-NSG mice, and even in NSG mice. Information about the spectrum of histopathological lesions occurring spontaneously in NSG mice is mainly limited to the prevalence of neoplastic findings in the NOD background strain[21] or a few reports on the most common causes of mortality and morbidity and age-related lesions in old NSG mice housed in conventional mouse facilities.[16,41] In the few reports available about hu-NSG mice, spontaneous changes were generally mentioned alongside the findings relevant to the study instead of being a focus of investigation.[8,30,41,54] However, a recent study reported histopathological lesions that provide evidence of the occurrence of graft versus host disease (GvHD) in HSC hu-NSG mice.[11] Considering the increasing use of humanized mice in efficacy and safety studies, including regulatory safety assessment, this knowledge gap needs to be addressed and better characterization of the model is warranted to consolidate its translatability.
The present study aimed to characterize the morphological phenotype of NSG mice and their humanized counterpart, the $CD34^+$ hu-NSG murine model generated via perinatal intrahepatic injection of human $CD34^+$ fetal liver cells into NSG mice after preconditioning irradiation. In addition, the histological features of the hemolymphatic organs were assessed, with particular emphasis on the presence and distribution of murine and human leukocytes, and the occurrence and prevalence of GvHD. We found high variability in the levels of human cell engraftment in the blood of hu-NSG mice within the same experiment and hypothesized that this is reflected by a similarly variable reconstitution in the lymphoid organs. In order to evaluate whether effective and non-effective engraftment would be reflected in the tissues we undertook a quantitative, morphometric immunophenotypic analysis on a representative group of mice that allowed an assessment of engraftment rates at *in situ* level and served to compare organ repopulation with blood reconstitution. Our results also provide evidence of GvHD as a relevant cause of morbidity and subclinical disease in this hu-NSG mouse model.

Materials and Methods

Animals

The study was undertaken on NOD-scid IL-2Rγ^{null} (NSG) mice from a breeding colony established in a research facility at the Institute of Experimental Immunology, University of Zurich, Switzerland from animals originally purchased from Jackson Laboratories (Bar Harbor, USA). Animals were housed in groups of up to five males or females respectively and fed ad libitum with conventional diet (M/R Haltung Extrudat, Alleinfuttermittel für Mäuse und Ratten, 3436; Granovit AG, Kaiseraugst, Switzerland). Water was provided *ad libitum*, the day and night cycle included 12 hours of light, from 6 am to 6 pm. The colony was maintained under specific pathogen-free conditions and sentinel animals were confirmed to be free of viral,

bacterial, and parasitic pathogens listed in the FELASA recommendations,[33] except for mouse norovirus (MNV) and *Helicobacter*.
The study cohort comprised a total of 109 mice. Among these were 48 NSG mice (31 males, 17 females) that did not receive any treatment. Of these, 10 (6 males, 4 females) were culled at 1-3 months of age, representing animals bred for, but not used in humanization experiments. Thirty-eight (25 males, 13 females) were breeding animals that were culled at 6 months of age, at the end of their breeding career. The second cohort of 61 hu-NSG mice (31 males, 30 females) were subjected to human cell engraftment and culled at the age of 3-5 months (deficiently humanized mice (n = 22; <15% $hCD45^+$ cells in peripheral blood after reconstitution): 3 months, efficiently humanized mice (n = 39): 4-5 months), at termination of an experiment to investigate the effects of Epstein-Barr virus infection on the immune system, in which they served as the non-infected control group. As part of the above-mentioned experiment on Epstein-Barr virus infection, the animals were injected intraperitoneally with 100 µl PBS at 12 to 14 weeks after irradiation. At the age of 4 months, 4 of these animals, 2 males and 2 females, developed progressive weight loss and signs of unease such as hunched posture, rough coat and reddened skin, and had to be euthanized. After reconstitution, mice were clinically checked daily for three days, and then three times a week until weaning. A weekly check was performed on mice four weeks and older, including naïve NSG mice.

Human Tissue Engraftment
$CD34^+$ HSC were isolated from fetal livers (Advanced Bioscience Resources, CA, USA) following established protocols.[46] Cells were frozen in liquid nitrogen prior to their use in the engraftment experiments. At the age of 1-6 days, NSG mice (n=61) were each irradiated with 1Gy (preconditioning), using a “Rad Source 2000” equipped with an X-ray source and injected intrahepatically 5-7 hours later with 1-$3x10^5$ $CD34^+$ human HSC. After 10-12 weeks, blood was collected via the tail vein and analyzed by FACS.

Ethics Statement
All animal protocols were in accordance with the Swiss Animal Welfare Act, Tierschutzgesetz (TSchG) and were approved by the veterinary office of the canton of Zurich, Switzerland (protocols 148/2011, 209/2014 and 159/17). The studies involving human samples were reviewed and approved by the cantonal ethics committee of Zurich, Switzerland (protocol KEK-StV-Nr.19/08, KEK-ZH-Nr. 2010-0057 and 2019-00837).

Macroscopic and Histological Examination
Mice were euthanized by 100% carbon dioxide asphyxiation, followed by exsanguination and creation of a pneumothorax. A full necropsy was conducted immediately after death on each mouse and a standard selection of organs, hemolymphatic tissues, as well as bones and joints were sampled and fixed in 10% neutral buffered formalin for 48-120 hours, then trimmed and routinely paraffin wax-embedded following a predefined blocking pattern. Consecutive sections (3-5 µm) were prepared and routinely stained with hematoxylin and eosin (HE), special stains (when appropriate) or subjected to immunohistochemical staining. Examined tissues were adrenal glands, brain, eyes, female genital tract (mammary gland, ovaries, uterus, vagina), gastrointestinal tract (stomach, duodenum, jejunum, ileum, cecum, colon and rectum), Harderian gland, heart, kidneys, liver with gall bladder, lungs, male genital tract (epididymis, prostate, testes, seminal vesicles), pancreas, salivary

glands, skeletal muscle (*Musculus quadriceps femoris*), skin, spinal cord, tongue, and urinary bladder. Examined hemolymphatic tissues were bone marrow from several locations (see bones), lymph nodes [cervical (one lymph node of the cervical chain: mandibular, accessory mandibular or superficial parotid), mesenteric (colic or jejunal), proper axillary] (in most animals, not all three lymph nodes were successfully sampled as these could not be identified grossly), spleen (1-2 cross sections), and thymus. Since thymus and lymph nodes were difficult to grossly identify especially in NSG mice, tissue in the corresponding area was collected and included in the paraffin block. Bones (sternum, femur and tibia with femorotibial joint, spinal column) as well as the head with nasal and oral cavities and teeth were also collected. After fixation, these were decalcified for 3-5 days in a mild decalcifying solution (RDF, Mild Decalcifier, CellPath, Newtown, UK), followed by paraffin embedding. Special stains were applied when considered necessary and comprised the Gram, Giemsa, Grocott, and Ziehl-Neelsen stains as well as the Periodic acid Schiff reaction).

Immunohistochemistry

Immunohistochemistry was applied to detect cells of human origin ($Ku80^+$), human and mouse leukocytes ($hCD45^+$, $mCD45^+$), T cells ($CD3^+$, $CD4^+$, $CD8^+$), human and mouse B cells ($CD45R\text{-}B220^+$ and $CD20^+$, respectively, monocytes/macrophages ($calprotectin^+$, $Iba1^+$, $F4/80^+$, $lysozyme^+$) and MHC II expression. Antibodies and detection methods are listed in Table 1A.

Table 1. Immunohistochemistry and FACS analysis

A. Antibodies and detection methods used for immunohistochemistry

Antigen	Cells detected (human, murine)	Antibody (clone)	Antigen retrieval	Detection method
hCD45	Human leukocytes	pAB rabbit anti-human CD45[a]	CB pH 6.0, 96°C, 30 min	1:500, 60 min, RT, HRP Envision Rb[e]
mCD45	Murine leukocytes	mAB rat anti-mouse CD45 (I3/2.3) [a]	CB pH 6.0, 96°C, 30 min	1:100, ON, RT, HRP Envision Rb[e]
Ku80	Human cells	mAB rabbit anti-human Ku80 (C48E7)[b]	TE pH 9.0, 96°C, 30 min	1:200, ON, 4 °C, HRP Envision. Rb[e]
Iba1	Human and murine macrophages	pAB rabbit anti-human Iba1[c]	CB pH 6.0, 96°C, 30 min	1:750, 60 min, RT, HRP Envision Rb[e]
F4/80	Mature murine macrophages	mAB rabbit anti-mouse F4/80 (SP115)[d]	TE pH 9.0, 96°C, 30 min	1:150, 2 h, 37 °C, Omni Ultra Map Kit Rb (Discovery)
Lysozyme	Human and murine macrophages, neutrophils	pAB rabbit anti-human lysozyme[e]	Proteinase K[e], RT, 5 min	1:400, 60min, RT, HRP Envision Rb[e]
CD45R	Murine B cells, reported to cross react with human	mAB rat anti-mouse CD45R/B220 (RA3-6B2)[f]	CB pH 6.0, 96°C, 30 min	1:800, 60 min, RT, HRP Envision Rb[e]
CD3	Human and murine T cells	mAB rabbit anti-mouse CD3 (SP7)[g]	TE pH 9.0, 96°C, 30 min	1:900, 1 h, 37 °C, Omni Ultra Map Kit Rb (Discovery)
Calprotectin	Human and murine granulocytes, monocytes, macrophages	mAB mouse anti-human S100A8/A9 (MAC387)[a]	CB pH 6.0, 96°C, 30 min	1:100, 30 min, RT, Omni Ultra Map Kit Rb (Discovery)
CD4	Human and murine T helper cells	mAB rabbit anti-mouse CD4 (EPR19514)[a]	CB pH 6.0 RT, 2 h	1:250, 1 h, RT, HRP Envision Rb[e]
CD8	Human and murine cytotoxic T cells	mAB rabbit anti-mouse CD8 (D4W2Z)[b]	CB pH 6.0 100°C, 20 min	1:50, 10 min, RT, Refine Detection Kit Mixed DAB[h]
CD20	Human and murine B cells	pAB rabbit[a]	CB pH 6.0 100°C, 20 min	1:400, 37°C, 1 h, Omni Ultra Map Kit Rb (Discovery)

Legend: mAB – monoclonal antibody; pAB – polyclonal antibody; CB – citrate buffer; TE – Tris-EDTA buffer; ON – overnight; RT – room temperature; Rb - rabbit
Commercial providers:
[a]Abcam, Cambridge, UK
[b]Cell Signaling Technology, Leiden, The Netherlands
[c]WAKO, Osaka, Japan
[d]Invitrogen/Thermo Fisher Scientific, Waltham, MA, USA
[e]Dako, Glastrup, Denmark
[f]BD Pharmigen, Franklin Lakes, USA
[g]Spring Bioscience, Ventana Medical Systems, Tucson, USA
[h]Leica Biosystems, Wetzlar, Germany

B. Antibodies applied in the FACS analysis to detect human cells.

Antigen	Cells detected	Antibody and fluorophore (clone)	Dilution
CD45	Leukocytes	mAB hCD45 Pacific Blue (HI30)[a]	1:500
CD3*	T cells	mAB CD3 PE (UCHT1)[a]	1:100
		mAB CD3 BV785(OKT3)[a]	1:100
CD4*	T helper cells	mAB CD4 APC-Cy7 (RPA-T4)[a]	1:100
		mAB CD4 BV605 (OKT4)[a]	1:100
CD8*	Cytotoxic T cells	mAB CD8 PerCP (SK1)[a]	1:100
HLA-DR*	Activated leukocytes	mAB HLA-DR FITC (L243)[a]	1:200
		mAB HLA-DR PE-Dazzle 594 (L243)[a]	1:200
CD19*	B cells	mAB CD19 Pe-Cy7 (HIB19)[a]	1:100
		mAB CD19 A700 (HIB19)[a]	1:50
NKp46*	NK cells	mAB NKp46 APC (9E2)[b]	1:100

Legend: mAB – mouse monoclonal antibody
*Analysis was conducted after gating for hCD45 in order to only include human cells for subsequent FACS analysis.
Commercial Providers:
[a]Biolegend, San Diego, USA
[b]BD Pharmigen Franklin Lakes, USA

Histological Scoring and Histomorphometry

All tissues/organs were examined for histopathological changes which were diagnosed following the International Harmonization of Nomenclature and Diagnostic Criteria (INHAND), Society of Toxicological Pathology (www.toxpath.org/inhand.asp). When appropriate, lesions were graded semi-quantitatively using a score from 1 to 5 (1 = minimal, 2 = mild, 3 = moderate, 4 = marked, 5 = severe).

For morphometric evaluation, slides with hemolymphatic tissue sections stained by immunohistochemistry were scanned using a digital slide scanner (NanoZoomer-XR C12000, Hamamatsu Photonics K.K., Iwata City, Japan), the Visiopharm Integrator System (Visiopharm, Hoersholm, Denmark) was used for the subsequent quantitative analysis. The mCD45 and hCD45 positive cell fraction areas and the number of Ku80 (nuclear marker) positive nuclei per high power field were calculated on consecutive sections. The mCD45 positive cell fraction area in hemolymphatic organs repopulated by human cells was calculated following subtraction of the hCD45 positive area from the total tissue area.

FACS Analysis
FACS served to identify hCD45$^+$, CD3$^+$, CD4$^+$, CD8$^+$, CD19$^+$, NKp46$^+$, CD4/DR$^+$, CD8/DR$^+$ populations and followed previously described protocols.[2]
Peripheral blood was collected from humanized mice 3 months after human cell engraftment by tail vein bleeding into heparin-containing tubes (Heparin-Na, Braun). After two rounds of red blood cell lysis, peripheral blood mononuclear cells (PBMCs) were washed with PBS and stained with fluorescence coupled antibodies for 20 minutes at 4 °C. Antibodies are listed in Table 1B. Subsequently, cells were fixed in 4% paraformaldehyde diluted in phosphate buffered saline (PBS) for 0 to 24 hours. Data was acquired on the BD FACSCanto II using DIVA software and analysed using FlowJo software Version 10.2. The cells were first gated for singlets, followed by hCD45.

Statistical Analysis
Statistical analysis was conducted using a Statistics Software (SPSS, 23). Correlation between FACS results and abundance of hCD45 positive cells in the lymphoid organ tissue sections was tested using Pearson test. Spearman's correlation analysis was used to study the relationship between GvHD and activated T cells. For this analysis, GvHD was divided in three categories as 0 = not present; 1 = mild GvHD, occurring with low severity and limited distribution; and 2 = severe GvHD, occurring with high severity and broad distribution. Statistical significance was evaluated using Mann-Whitney-U-Test and t-test. p values <0.05 were considered statistically significant.

Results

Spontaneous background lesions in NSG and hu-NSG mice, radiation-induced changes in hu-NSG mice
The NSG mouse cohort (n = 48) remained healthy during the examination period and exhibited only a limited selection of histopathological lesions, with generally low severity (Table 2A). The most frequently encountered changes were minimal or mild multifocal alveolar macrophage accumulation with pleural thickening in the lungs; minimal focal tubular basophilia and tubular dilation with epithelial cell hypertrophy in the kidneys; minimal or mild patchy degeneration and dystrophic mineralization of seminiferous tubules in the testes; and minimal to moderate multifocal subcapsular cell hyperplasia in the adrenal glands. The latter occurred with higher frequency in females. Sporadically, minimal or mild focal degenerative changes in the intersternebral and intervertebral joints as well as cortical thickening of the femoral diaphysis were noted. Individual animals exhibited inflammatory processes, such as minimal focal neutrophilic myositis in retro-orbital and masticatory muscles, focal neutrophilic folliculitis in the skin of the muzzle, and a moderate diffuse chronic sialoadenitis. The latter appeared to be the consequence of an obstruction of the main excretory duct by a hair. Also, one mouse showed marked chronic pancreatitis, characterized by diffuse fibrosis, moderate mononuclear cell inflammation and lobular acinar atrophy. Apart from occasional dilation of endometrial glands, the female reproductive tract was free of histopathological changes. Ovaries exhibited numerous follicles at different stages of maturation and corpora lutea and the vagina showed normal cyclic changes consistent with all four phases of the rodent reproductive cycle.

Table 2. Spectrum of histopathological lesions in male and female NSG and hu-NSG mice

A. NSG mice, aged 1-3 months (n=10) and 6 months (n=38)

Organs (alphabetical order) and histological findings	Males	Females
Adrenal glands		
Subcapsular cell hyperplasia	18% (5/28)	69% (11/16)
Extramedullary hematopoiesis	7% (2/28)	-
Angiectasis (corticomedullary junction)	-	13% (2/16)
Accessory cortical tissue	-	13% (2/16)
Bones and joint		
Intersternebral joint degeneration	4% (1/28)	-
Femoral articular cartilage degeneration (clefts)	10% (3/30)	-
Intervertebral joint degeneration	3% (1/30)	-
Focal cortical thickening of femoral diaphysis	10% (3/30)	7% (1/15)
Bone marrow (sternum and femur)		
Hemosiderosis	19% (6/31)	40% (6/15)
Fatty infiltration (femur only)	17% (5/30)	73% (11/15)
Myeloid hyperplasia	3% (1/31)	-
Kidneys		
Tubular dilation with epithelial cell hypertrophy	13% (4/31)	6% (1/17)
Tubular basophilia	6% (2/31)	6% (1/17)
Lungs		
Alveolar macrophage aggregation with pleural thickening	77% (24/31)	65% (11/17)
Hair shaft granuloma	3% (1/31)	-
Pancreas		
Acinar atrophy with chronic inflammation	3% (1/31)	-
Salivary gland (submandibular)		
Chronic inflammation, due to foreign body (hair)	-	6% (1/17)
Skeletal muscle		
Myofibre degeneration with inflammation, retroorbital muscle	-	6% (1/17)
Myofibre degeneration with inflammation, masticatory muscle	3% (1/31)	-
Skin (muzzle)		
Neutrophilic inflammation, hair follicle	-	6% (1/17)
Spleen		
Extramedullary hematopoiesis	100% (31/31)	100% (15/15)
Hemosiderosis	32% (10/31)	80% (12/15)
Testes		
Seminiferous tubule degeneration with mineralization	42% (13/31)	
Thymus		
Cysts	56% (9/16)	62% (8/13)
Thymus/mediastinal lymph node*		
Precursor T cell lymphoblastic lymphoma	-	8% (1/13)
Uterus		
Glandular dilation with luminal debris		29% (5/17)

*: Tissue of origin could not be determined

The hu-NSG mice exhibited the same type of background lesions as the NSG mice, and with similar frequency and severity (Table 2B). In addition, hu-NSG mice showed histological changes consistent with exposure to radiation in the early postnatal period, i.e. radiation nephropathy, cataract and impaired retinal development in the eye,[4] and ovarian atrophy.[1,6] Evidence of radiation nephropathy (deposition of proteinaceous material and reduced number of capillaries in glomeruli, cortical tubular collapse[36]) was observed in relatively few mice (13% of males, 17% of females), and with minimal severity (Figs. 1, 2). Impaired retinal development was far more frequent (more than 70% of animals). It ranged from a thinning of the outer nuclear layer and the outer segment layer, to a lack of distinction between outer and inner nuclear layer, leading to a very thin retina composed of a single row of nuclei (Figs. 3, 4). Changes were more severe in the peripheral portion of the retina. Cataract occurred in fewer mice (Table 2B) with low severity. Almost all female animals exhibited ovarian atrophy, and of varying degree. In more severe cases, the ovaries were reduced in size and exhibited a marked reduction to complete absence of oocytes, follicles and corpora lutea (Figs. 5, 6). Such animals appeared to be in persistent anestrus, as there was no evidence of normal estrus cycling in uterus and vagina.

B. Hu-NSG mice, aged 3-6 months (n=61)

Organs (alphabetical order) and histological findings	Males	Females
Adrenal glands		
Subcapsular cell hyperplasia	45% (10/22)	96% (24/25)
Angiectasis (corticomedullary junction)	-	16% (4/25)
Accessory cortical tissue	4.5% (1/22)	8% (2/25)
Bones and joint		
Femoral articular cartilage degeneration (clefts)	-	7% (1/15)
Bone marrow (sternum and femur)		
Fatty infiltration (femur only)	29% (4/14)	53% (8/15)
Myeloid hyperplasia	4% (1/27)	4% (1/28)
Granulomatous inflammation (human cells)*	30% (8/27)	14% (4/28)
Eyes		
Impaired retinal development	73% (16/22)	75% (18/24)
Cataract	14% (3/22)	4% (1/24)
Kidneys		
Tubular dilation with epithelial cell hypertrophy	6% (2/31)	3% (1/30)
Tubular basophilia	-	10% (3/30)
Radiation nephropathy	13% (4/31)	17% (5/30)
Granulomatous inflammation (human cells)*	6% (2/31)	7% (2/30)
Liver		
Multifocal lymphohistiocytic cell aggregates (human cells)*	26% (8/31)	17% (5/30)
Granulomatous inflammation (human cells)*	16% (5/31)	17% (5/30)
Extramedullary haematopoiesis	23% (7/31)	27% (8/30)
Focal hepatocellular necrosis	3% (1/31)	-
Lungs		
Alveolar macrophage aggregation with pleural thickening	94% (29/31)	87% (26/30)
Multifocal lymphohistiocytic cell aggregates (human cells)* with alveolar hemorrhage and fibrin deposition	29% (9/31)	13% (4/30)
Ovaries		
Atrophy	-	89% (24/27)
Pancreas		
Acinar atrophy with chronic inflammation	5% (1/22)	-
Multifocal lymphohistiocytic cell aggregates (human cells)*	5% (1/22)	8% (2/24)
Salivary gland		
Acinar atrophy with chronic inflammation (mandibular gland)	5% (1/22)	-
Skeletal muscle		
Myofiber degeneration with inflammation, masticatory muscle	5% (1/21)	-
Skin		
Interface dermatitis with scleroderma	21% (4/19)	-
Spleen		
Extramedullary hematopoiesis	97% (28/29)	100% (29/29)
Hemosiderosis	3% (1/29)	31% (9/29)
Granulomatous inflammation (human cells)*	10% (3/29)	10% (3/29)
Testes		
Seminiferous tubule degeneration with mineralization	45% (10/22)	
Thymus		
Cysts	47% (7/15)	47% (7/15)

*: Ku80-positive infiltrates, considered as graft versus host disease (GvHD); see also Table 3.

Numbers in parenthesis represent the number of animals exhibiting the specific lesion over the number of examined animals

Figures 1-6. Histological changes in hu-NSG mice caused by exposure to radiations.

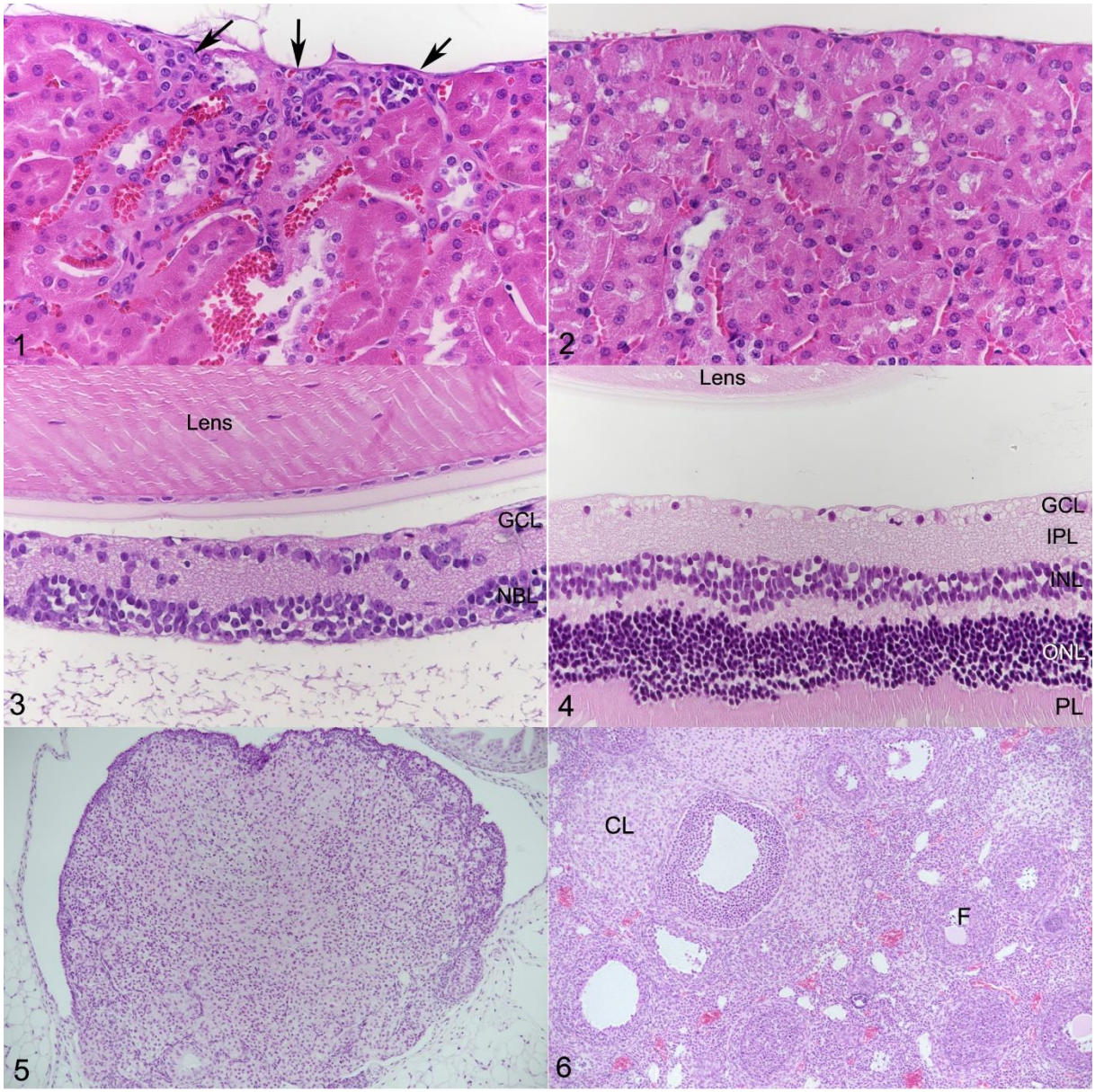

Figure 1. Kidney, hu-NSG mouse. Radiation nephropathy, characterized by cortical tubular collapse (arrows). **Figure 2**. Kidney, NSG mouse, without histological changes. **Figure 3**. Eye, hu-NSG mouse. Impaired retinal development. Most normal structures of the retina cannot be identified. There appears to be an irregular ganglion cell layer (GCL) and a defined neuroblastic layer (NBL) of up to six cell layers. **Figure 4**. Eye, NSG mouse. The retina is unaltered. GCL - ganglion cell layer, IPL - inner plexiform layer, INL- inner nuclear layer, ONL - outer nuclear layer, PL - photoreceptor layer. **Figure 5**. Ovary, hu-NSG mouse. Ovarian atrophy. The ovary is very small and devoid of follicles and corpora lutea. **Figure 6**. Ovary, NSG mouse. Functional ovary with numerous oocytes, follicles (F) and corpora lutea (CL). HE stains.

Hemolymphatic tissues

Spleens, lymph node, thymus and bone marrow were compared in both groups of mice, in particular to comparatively assess the murine and human leukocyte component in hu-NSG mice. Based on previous experience of the group, hu-NSG mice were classified as deficiently humanized (hu-NSG(d) mice), when they exhibited less than 15% $hCD45^+$ cells in the blood (determined by FACS). This applied to 39.9% (22/61) of the animals in the present study.

Spleen. In NSG mice, spleens were generally small, less than 12 x 2 x 1 mm in size, with rare, randomly distributed leukocytes ($mCD45^+$) and no morphological evidence of lymphocytes populating follicles and T cell zones. Interestingly, in more than half (27/48) of the mice, small aggregates of $mCD45^+$ cells were found around one or two arterioles, reminiscent of periarteriolar lymphoid sheaths (PALS; Fig. 7a, b). The aggregates were composed of round to polygonal cells of approximately 15 µm in diameter, with very scant cytoplasm and a large round to slightly elongated nucleus with finely stippled chromatin and no evident nucleolus. These cells were consistently negative for T cell (CD3), B cell (CD45R-B220) and macrophage (F4/80, calprotectin and lysozyme) markers. The red pulp was mainly populated by erythroid progenitors and some megakaryocytes, representing minimal to moderate extramedullary hematopoiesis (Fig. 7a), and scattered leukocytes; some animals also exhibited minimal hemosiderosis.

Spleens were substantially larger In all hu-NSG mice, measuring approximately 15 x 5 x 2 mm on average. Histology showed that this was due to the much higher cellularity of the organ secondary to human cell repopulation. While there was no evidence of follicular structures, human cells tended to cluster around splenic arterioles, forming PALS-like structures (Fig. 8) similar to but generally much larger than those formed occasionally by $mCD45^+$ cells in the spleen of NSG mice. In the latter, due to the PAL-like aggregates, the proportion of the area in the spleen covered by $mCD45^+$ cells exceeded 10% in some animals (n = 6; mean = 6.3; SD = ±7.8) (Fig. 9), whereas murine leukocytes ($mCD45^+$) were extremely rare in hu-NSG mice (Figs. 8b, 9). In contrast, they carried numerous $hCD45^+$ cells (Fig. 8c). In efficiently humanized (hu-NSG(e)) mice, the hCD45 positive cell fraction area was 21.0% on average, though the proportion varied considerably between animals (Table 3). In deficiently humanized mice, the hCD45 positive cell fraction area had a mean of 8.8% (Table 3); however, the difference between the two groups was not significant. The white pulp in hu-NSG mice consisted of B cells ($CD20^+$) and T cells ($CD3^+$) in equal proportions. The T cells were mostly found in the center of the reconstituted white pulp, in the PALS-like structures around the arteries (Fig. 10a); B cells tended to occupy the periphery of the white pulp but did not arrange in clear follicular structures (Fig. 10b). Staining for CD4 and CD8 identified mainly $CD4^+$ T cells whereas only random individual cells scattered throughout the parenchyma were found to be $CD8^+$. In all animals, the remaining area (red pulp) was mainly occupied by erythroid progenitor cells, intermingled with megakaryocytes (moderate extramedullary hematopoiesis) (Fig. 8a) and scattered $hCD45^+$ leukocytes with the morphology of lymphocytes; these appeared to be represented by B cells and T cells in equal proportions (Fig. 10).

Figures 7-10. Morphology and composition of the spleen in NSG and hu-NSG mice.

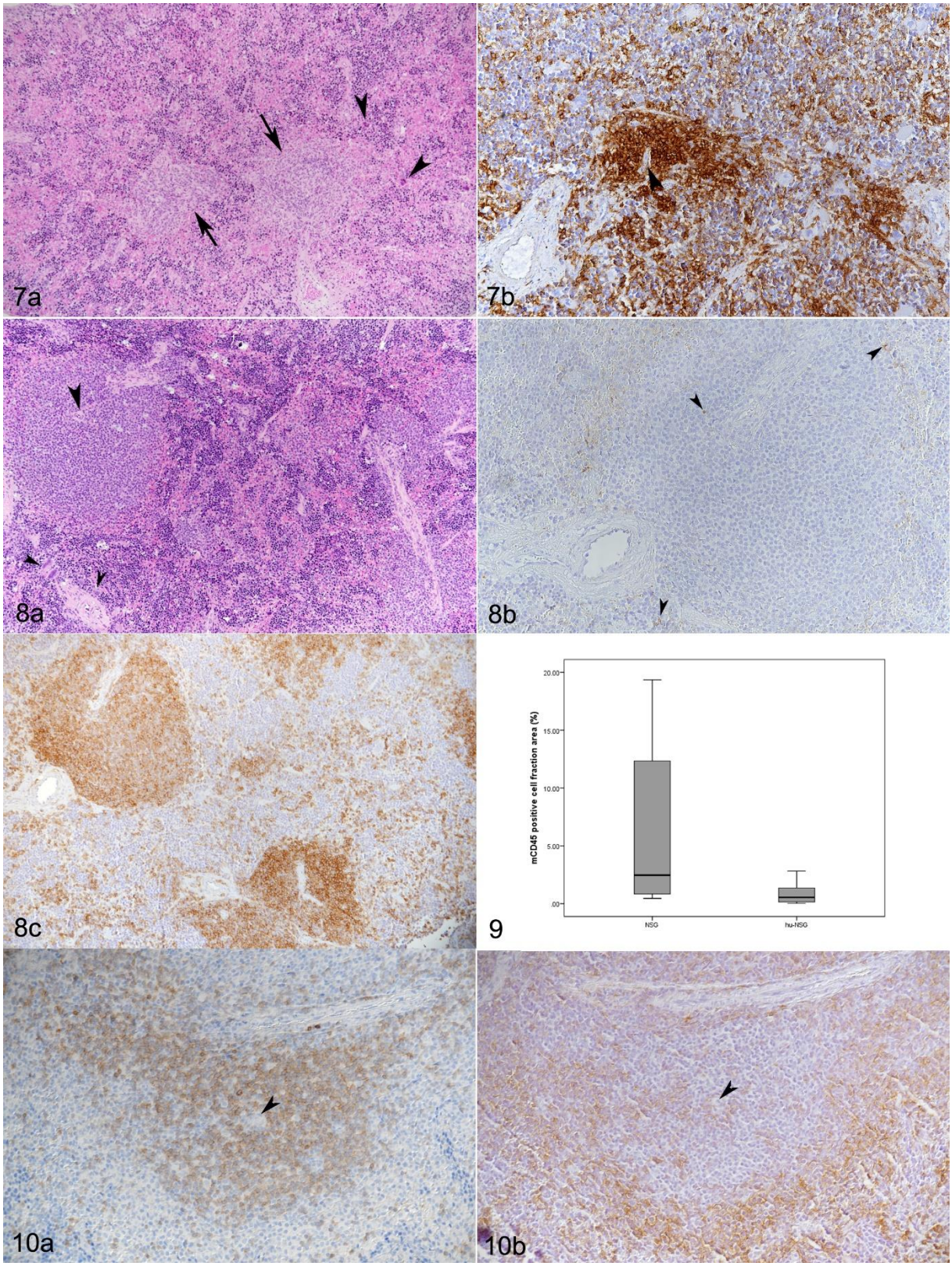

Figure 7. NSG mouse. **a**. There are no distinct white pulp structures. Occasional aggregates of round cells form structures reminiscent of periarteriolar lymphoid sheaths (PALS) (arrows). The red pulp is cell rich, mainly due to extramedullary hematopoiesis (arrowheads: megakaryocytes). HE stain. **b**. The PALS-like structures are comprised of $mCD45^+$ cells that aggregate around a splenic arteriole (arrowhead). Numerous $mCD45^+$ cells are also seen randomly distributed in the red pulp. Immunohistochemistry, hemalaun counterstain. **Figure 8**. hu-NSG mouse. **a**. The white pulp is evident by large aggregates of lymphoid cells clustering around arterioles (large arrowhead), consistent with PALS. The red pulp is cell rich, with abundant extramedullary hematopoiesis (small arrowheads: megakaryocytes). HE stain. **b**. Murine leukocytes ($mCD45^+$) are very rare (arrowheads).

Immunohistochemistry, hemalaun counterstain. **c**. Human leukocytes (hCD45$^+$) form the PALS-like aggregates and are also distributed in moderate number throughout the red pulp (hCD45 positive cell fraction area of 13.4%). Immunohistochemistry, hemalaun counterstain. **Figure 9**. Boxplot presenting the area in the spleen of NSG and hu-NSG mice covered by mCD45$^+$ cells (mCD45 positive cell fraction area in %). There is a trend towards a lower percentage of mCD45$^+$ cells in hu-NSG mice, however, the difference is not statistically significant ($p = 0.148$). **Figure 10**. hu-NSG mouse. **a**. The PALS-like structures around the arteries (arrowhead) are mainly comprised of T cells (CD3$^+$). **b**. B cells (CD20$^+$) arrange around the PALS-like structures, without forming clear follicles. Immunohistochemistry, hemalaun counterstain.

Lymph nodes. In NSG mice, lymph nodes were generally very small and difficult to identify grossly, however, in the majority of animals, the mesenteric and mandibular lymph nodes were successfully sampled. They were composed predominantly of connective tissue, i.e. the reticular stroma (Fig. 11a, b). Leukocytes (mCD45$^+$) were present in low numbers, scattered throughout the fibrous scaffold (Fig. 11c, d). When sampled successfully, axillary and inguinal lymph nodes exhibited the same morphological features.

Lymph nodes of hu-NSG mice were in general larger and therefore easier to identify grossly. Histologically, most lymph nodes were abundantly populated by lymphoid round cells (Fig. 12). They contained only few murine leukocytes (mCD45$^+$; $n = 33$, mean = 0.86%, SD = ±1.8), and on average less than the lymph nodes of NSG mice ($n = 11$; mean = 2.8; SD = ±4.1) (Fig. 13). Instead, human leukocytes (hCD45$^+$) repopulated the fibrous stroma ($n = 33$; mean = 42.1%; SD = ±22.4) (Fig. 12d). In efficiently humanized mice, the hCD45 positive cell fraction area had a mean of 54.1%, whereas in deficiently humanized mice, the mean was 18.6% (Table 3). In some of the latter animals no human cells were identified at all; these lymph nodes had morphological features identical to those of the NSG mice. However, also in the efficiently humanized mice, repopulating hCD45$^+$ cells appeared to distribute randomly across the lymph node, did not aggregate to form appreciable lymphoid follicles or paracortical structures, and did not allow corticomedullary distinction. Accordingly, CD20$^+$ B cells which were present in moderate to high numbers, and CD3$^+$ T cells which were slightly less numerous, were seen randomly distributed throughout the stroma. Overall, the periphery had a higher proportion of B cells (Fig. 12b) while T cells tended to be more numerous in the center (Fig. 12c). Most T cells appeared to be CD4$^+$, whereas CD8$^+$ cells were only present in very small numbers.

Figures 11-13. Morphology and composition of lymph nodes in NSG and hu-NSG mice.

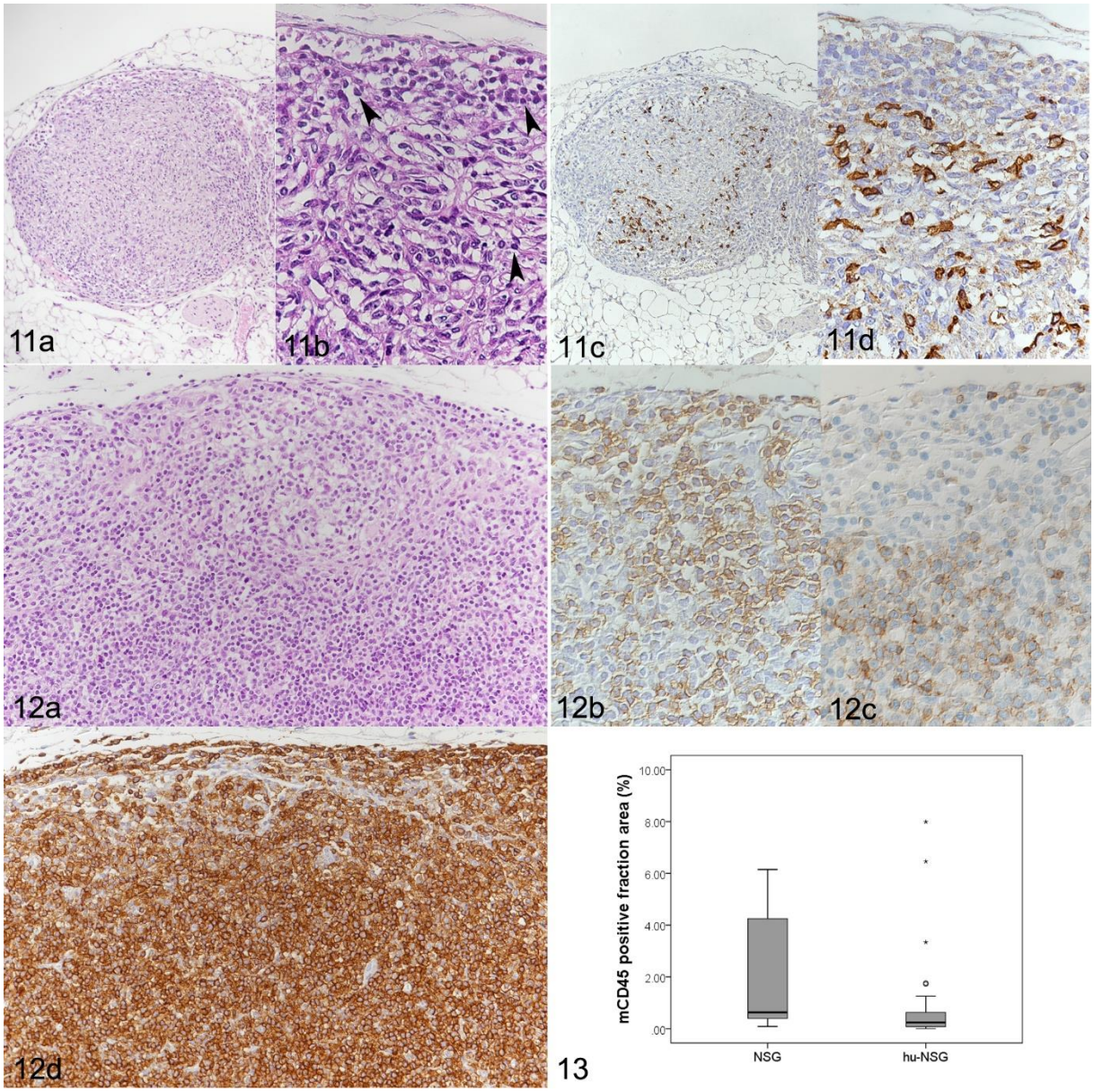

Figure 11. Mesenteric lymph node, NSG mouse. **a**. Overview of the very small lymph node. **b**. The higher magnification shows that it is mainly represented by a meshwork of fibrous tissue (reticular stroma), with low numbers of embedded leukocytes (arrowheads). HE stains. **c**. Staining for mCD45$^+$ confirms the low number of leukocytes. **d**. Higher magnification. Immunohistochemistry, hemalaun counterstain. **Figure 12**. Mesenteric lymph node, hu-NSG mouse (well repopulated; hCD45 positive cell fraction area of 43.2%). **a**. The lymph node exhibits high cellularity, although no clear follicular and paracortical structures are identified. HE stain. **b**. The repopulating cells are B cells (CD20$^+$) and **c**. T cells (CD3$^+$) that seem to cluster to some extent but do not form follicles or T cell zones. **d**. Almost all cells are hCD45 positive. Immunohistochemistry, hemalaun counterstain. **Figure 13**. Boxplot presenting the area in the lymph nodes of NSG and hu-NSG mice covered by mCD45$^+$ cells (mCD45 positive cell fraction area in %). There is a trend towards a lower percentage of mCD45$^+$ cells in hu-NSG mice, however, this is not statistically significant (p = 0.059).

Thymus. In NSG mice, the thymus was generally barely visible and composed of hypoplastic lobules that lacked a defined cortex and medulla and often contained cysts, as previously reported (Fig. 14).[7] Again, leukocytes (mCD45$^+$) were rare (Fig. 15).

The thymus generally appeared slightly larger in hu-NSG mice, with an approximate size of 2 x 1 x 1 mm. Lobules were more cellular and exhibited moderate numbers of lymphoid cells (Fig. 16), but still lacked the typical corticomedullary distinction. Murine leukocytes were rare, the mCD45 positive cell fraction area had a mean of 0.4 %

(Fig. 17). Still, mCD45+ cells were sometimes more numerous than in NSG mice, where the area covered by $mCD45^+$ cells did not exceed 0.3% (n = 9; mean = 0.09; SD = ±0.1) (Fig. 17). Repopulation with $hCD45^+$ leukocytes was variable in hu-NSG mice. In efficiently humanized mice, the mean of the hCD45 positive cell fraction area reached 46.1%, whereas it was 16.5% in deficiently humanized mice (Table 3). The majority of these cells were $CD3^+$. Of this subpopulation most cells were $CD4^+$ whereas $CD8^+$ cells were only visible in very small numbers. $CD20^+$ cells were barely present.

Figures 14-17. Morphology and composition of the thymus in NSG and hu-NSG mice.

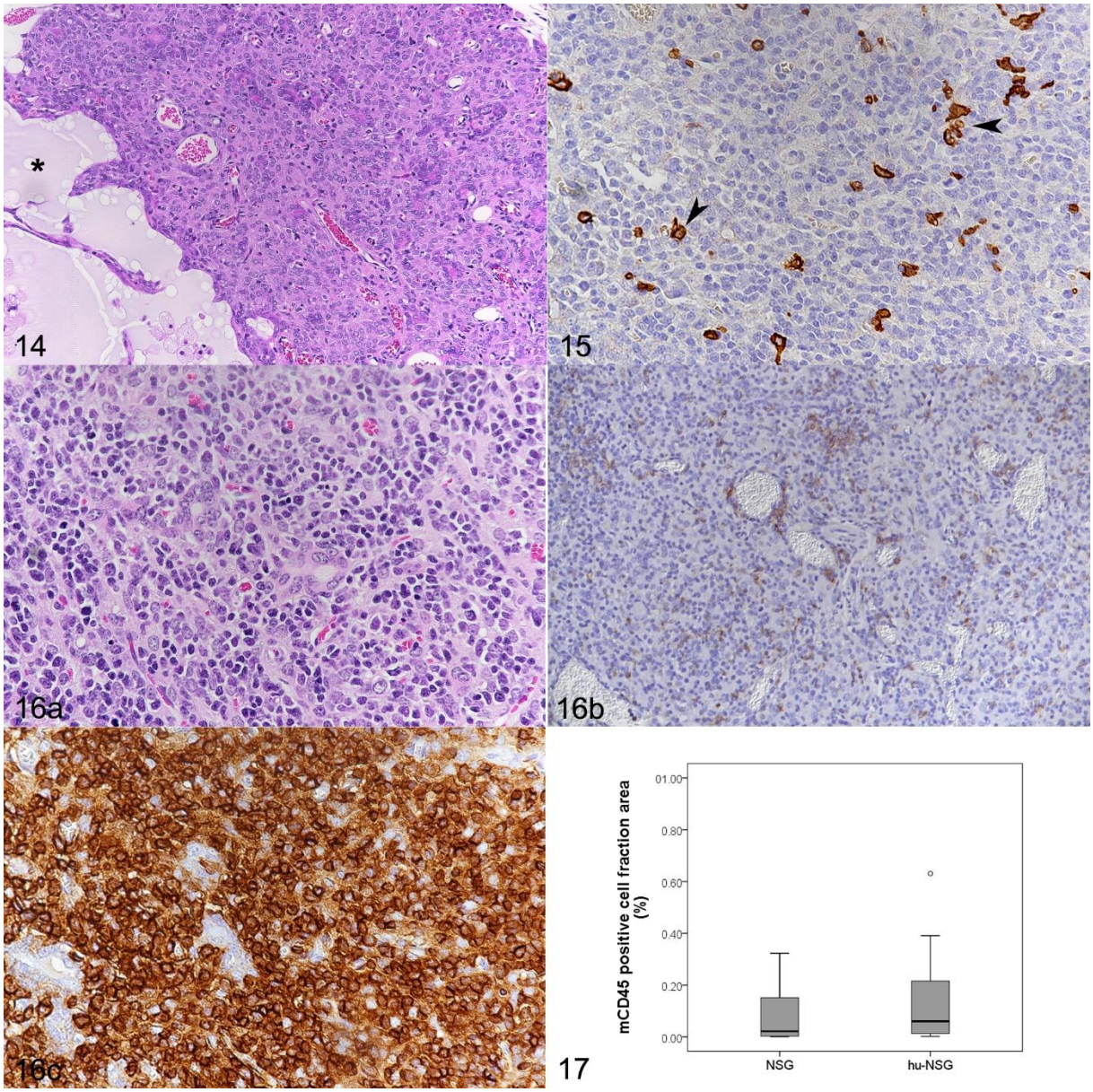

Figures 14, 15. NSG mouse. **Figure 14**. Hypoplastic thymus without defined cortex and medulla, devoid of lymphocytes and with a large cyst (*). HE stain. **Figure 15**. Leukocytes ($mCD45^+$) are found in low numbers and randomly distributed (arrowheads). Immunohistochemistry, hemalaun counterstain. **Figure 16**. hu-NSG mouse. **a**. Cortex and medulla cannot be identified, but there is a moderate cellularity with numerous disseminated lymphoid round cells. HE stain. **b**. Murine leukocytes ($mCD45^+$) are found disseminated and in low numbers. **c**. The vast majority of the round cells are $hCD45^+$ human leukocytes, confirming repopulation (hCD45 positive cell fraction area of 42.6%). Immunohistochemistry, hemalaun counterstain. **Figure 17**. Boxplot presenting the area in the thymus of NSG and hu-NSG mice covered by $mCD45^+$ cells (mCD45 positive cell fraction area in %). There is no significant difference in the percentage of $mCD45^+$ cells between the two groups of mice (p = 0.533).

One 6-month-old female breeding NSG mouse exhibited a white-tan, firm mass of approximately 0.4 cm in diameter in the thoracic cavity. Histologically, it was composed of dense sheets of large round neoplastic cells which also infiltrated the adjacent adipose tissue (Fig. 18). The cells exhibited scant amphophilic cytoplasm and round nuclei with coarsely arranged chromatin. There was moderate anisocytosis and a mitotic rate of 2-4/HPF; a moderate number of apoptotic cells was observed (Fig. 19a). The vast majority of cells were found to express CD3 and CD4 (Fig. 19 b, c), whereas B cells ($CD45R^+$) were seen in low numbers and randomly distributed. This led to the diagnosis of a precursor T cell lymphoblastic lymphoma.[34] It was not possible to determine whether the neoplasia originated from the thymus or the mediastinal lymph nodes. The mouse did not exhibit further neoplastic masses or any other histopathological changes.

Figures 18, 19. T cell lymphoblastic lymphoma, thoracic cavity, NSG mouse, 6 months, female.

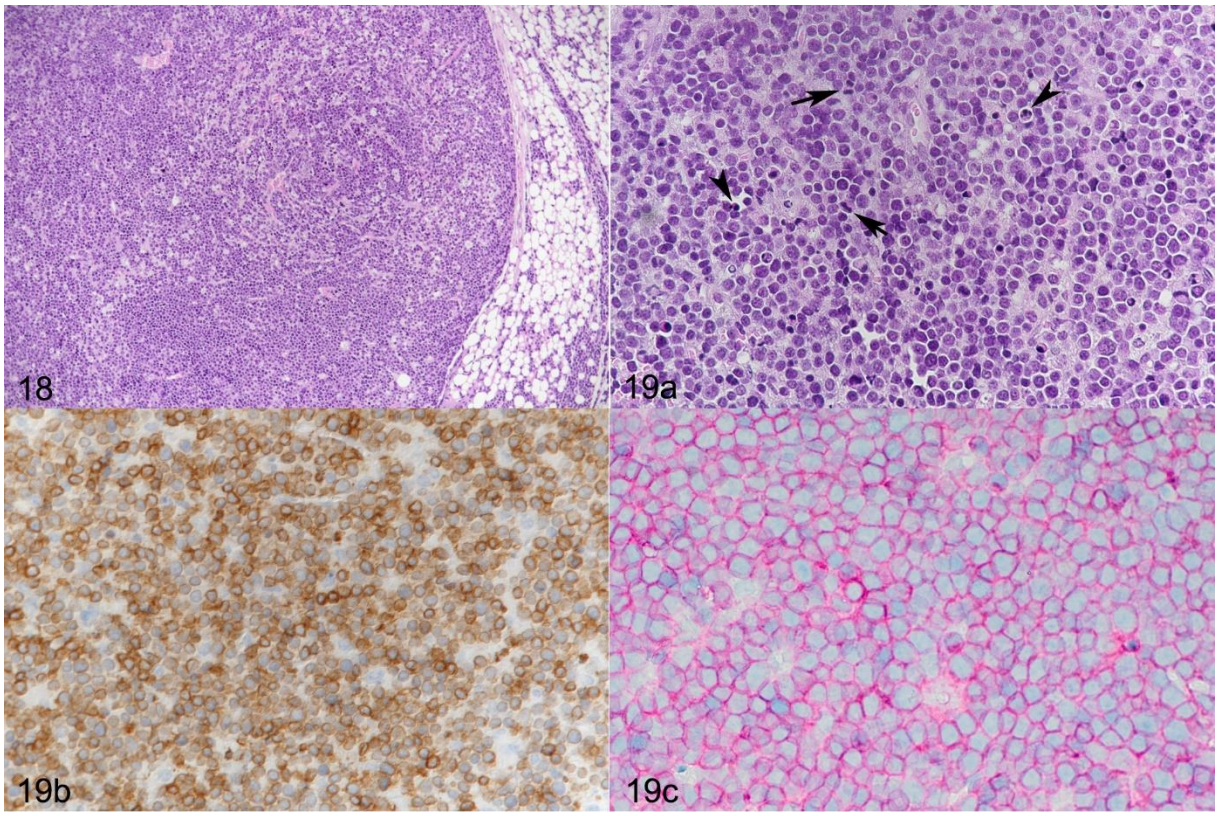

Figure 18. Thoracic mass composed of a monomorphic neoplastic cell population that also infiltrates the adjacent mediastinal adipose tissue. HE stain. **Figure 19**. **a**. Neoplastic cells are arranged in tightly packed sheets and display scant amphophilic cytoplasm, round nuclei with coarsely arranged chromatin, and moderate anisocytosis. There are several mitotic (arrows) and apoptotic (arrowheads) cells. HE stain. **b**. The vast majority of neoplastic cells express the pan T cell marker CD3. **c**. Neoplastic cells are also CD4 positive (pink reaction along the cell border), but CD8 negative (blue reaction along the cell border). Immunohistochemistry, hemalaun counterstain.

Bone marrow. In NSG mice, the bone marrow (sternal and femoral) generally exhibited a high cellularity, represented by erythroid, $mCD45^+$ myeloid and megakaryocytic hematopoietic precursors (Fig. 20). Mild to moderate hemosiderosis as well as fatty infiltration (femur only) was occasionally seen (Table 2A).

In hu-NSG mice, the morphology of the bone marrow was similar, with high cellularity (Fig. 21). While $mCD45^+$ cells were very rare, making up a significantly lower proportion of area than in the NSG mice (Fig. 21), $hCD45^+$ cells were the dominant

cell population (Fig. 21c). A comparison of the number of human cells (Ku80^{+}) in efficiently and deficiently humanized mice revealed a significantly higher proportion of human cells in efficiently humanized mice (Table 3).

Figures 20-22. Morphology and composition of the femoral bone marrow in NSG and hu-NSG mice.

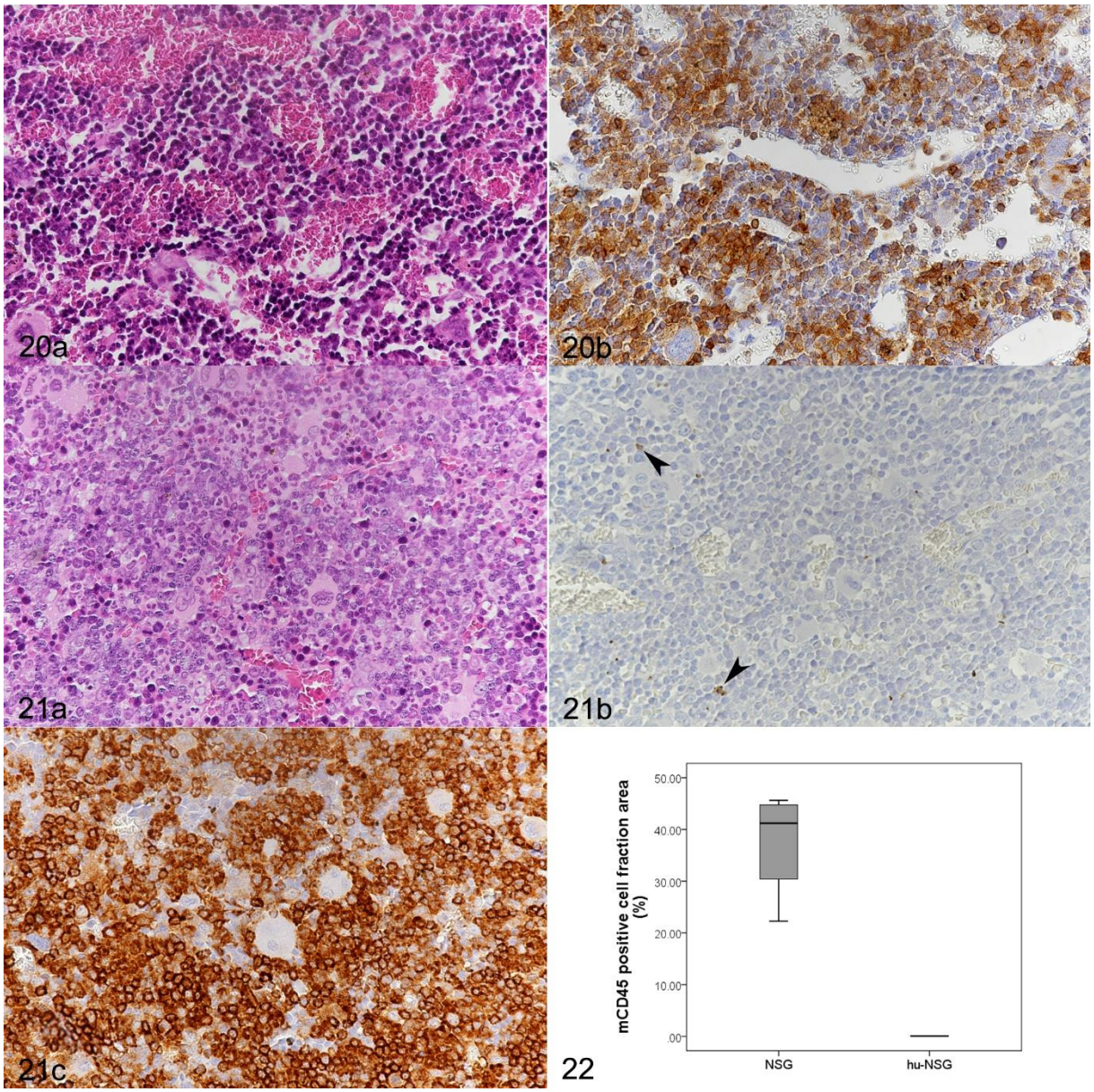

Figure 20. NSG mouse. **a**. The bone marrow is cell rich; all hematopoietic cells are represented. HE stain. **b**. There are abundant mCD45^{+} leukocytes. Immunohistochemistry, hemalaun counterstain. **Figure 21**. hu-NSG mouse. **a**. The bone marrow is highly cellular; all hematopoietic cell lineages are represented. HE stain. **b**. The number of mCD45^{+} cells is extremely low, positive cells are often apoptotic (arrowheads). **c**. The vast majority of cells are hCD45^{+} leukocytes. Immunohistochemistry, hemalaun counterstain. **Figure 22**. Boxplot presenting the area in the bone marrow of NSG and hu-NSG mice covered by mCD45^{+} cells (mCD45 cell fraction area in %). A statistically significant ($p = 0.006$) lower percentage of mCD45^{+} cells is present in hu-NSG mice.

Table 3. Human cells in the lymphoid organs of efficiently humanized NSG mice (hu-NSG mice; animals with more than 15% hCD45 cells in the blood at the age of three months) and deficiently humanized NSG mice (hu-NSG(d) mice; animals with less than 15% hCD45 cells in the blood at the age of three months). The area covered by human cells (hCD45+) in spleen, lymph nodes, thymus, and the number of Ku80-positive human cells in the bone marrow was measured. Significant differences were tested between hu-NSG and hu-NSG(d) using t test.

Organ	**Hu-NSG (n=8)**			**Hu-NSG(d) (n=8)**			
	Range (%)	**Mean (%)**	**SD ±**	**Range (%)**	**Mean (%)**	**SD±**	**P-value**
Spleen	8.4 - 46.8	21.0	13.9	0.1 - 35.5	8.8	12.8	p = 0.87
Lnn[a]	41.8 - 59.5	54.1	6.5	0.0 - 51.2	18.6	24.3	**p = 0.008**
Thymus	27.9 - 65.2	46.1	11.8	0.0 - 65.2	16.5	27.5	**p = 0.030**
BM[b]	42.3 - 88.4	69.6	15.0	0.5 - 56.3	28.2	23.3	**p = 0.001**

Lnn - lymph nodes; BM - bone marrow
[a]The mean of hCD45+ area of the detected, i.e. histologically examined lymph nodes in each animal was taken for the calculation.
[b]hu-NSG mice: n = 12; hu-NSG(d) mice: n = 4
Significant values are highlighted in bold.

Graft versus host disease (GvHD) in CD34$^+$ hu-NSG mice

Two male and two female hu-NSG mice developed poor health before study completion and were electively euthanized, the females at 28 weeks after HSC transplantation due to severe progressive weight loss, and the males at 30 weeks. Both were thin and had exhibited signs of unease such as hunched posture, rough coat and reddened skin. All four mice exhibited grossly enlarged lymph nodes and spleen, a diffusely pale bone marrow, and a red and white mottled liver. The histological examination revealed extensive granulomatous inflammatory infiltrates in these tissues as well as in the kidneys (Figs. 23-29). There was no evidence of bacterial or fungal organisms within the inflammatory infiltrates, as confirmed by various special stains (Gram, Giemsa, Periodic acid Schiff, Grocott, and Ziehl-Neelsen). Therefore, the inflammatory processes were considered a manifestation of GvHD.[11,45] They were represented by multifocal to coalescing, partly nodular aggregates of macrophages and epithelioid cells, admixed with numerous lymphoid and multinucleated giant cells (Figs. 23-29). In the infiltrates, cells were often found to proliferate, which was reflected by the presence of mitotic cells (1-3 mitotic figures per high power field). The vast majority of cells were human leukocytes (Ku80$^+$ (Fig. 24b), hCD45$^+$), with only very few intermingled murine (mCD45$^+$) leukocytes. Macrophages and T cells (CD3$^+$) dominated in the infiltrates which also contained a variable portion of B cells and a few viable neutrophils (Fig. 24c, d). A combined immunohistochemical stain for CD4 and CD8 antigens revealed a striking predominance of CD4$^+$ T cells, with only rare CD8 or double positive cells. In the liver, GvHD consisted of lymphohistiocytic or granulomatous infiltrates that were mainly located in periportal areas (Figs. 23, 24a) and were associated with minimal to moderate deposition of fibrous connective tissue as well as scattered hemosiderin-laden macrophages. Bile ducts were often embedded within the inflammatory reaction, but were neither altered nor infiltrated, suggesting that they were not targeted by the inflammatory cells at this stage. Bone marrow affection was represented by scattered nodules randomly distributed in the hematopoietic tissue (Fig. 25a) to subtotal replacement of the hematopoietic cell component by, in the majority, MHC II positive cells (Fig. 25b), with concurrent bone marrow necrosis and hemorrhage as well as bone resorption. Affected spleens and lymph nodes (Figs. 26-29) showed scattered focal infiltrates or severe disruption of the architecture by the inflammatory infiltrates. When affected, kidneys exhibited only mild changes, represented by scattered granulomatous foci randomly distributed throughout the cortical interstitium. In individual cases, pancreas, ovaries, serosae, Harderian glands, nose and/or oral cavity also showed granulomatous infiltrates.

Some animals with the above-described GvHD lesions also exhibited inflammatory infiltrates in lungs and skin. In the lungs, these represented peribronchiolar and perivascular aggregates of Ku80-positive cells, which were predominantly T cells and B cells, with fewer macrophages. Infiltrates occasionally extended into the bronchiolar and alveolar lumina. In the skin, minimal or mild infiltration of Ku80-positive, predominantly CD4$^+$ and fewer CD8$^+$ T cells and rare B cells was seen along the dermo-epidermal junction, associated with vacuolar change and occasional apoptosis in the basal follicular keratinocytes and, to a lesser extent, the basal epidermal keratinocytes.

Granulomatous inflammatory infiltrates were also observed in other mice, with lower severity and higher incidence in males (21%; 6/29) than in females (11%; 3/28). Liver, spleen, lymph nodes, bone marrow at different locations (sternum, femur and tibia, vertebrae and frontal bones in the skull) and kidneys were most consistently affected (Table 4).

Table 4. Incidence and severity of granulomatous and/or mononuclear inflammatory infiltration (mediated by human cells) in the organs of hu-NSG mice.

Organ	Sex	Granulomatous inflammatory infiltration				
		Minimal	Mild	Moderate	Marked	Severe
Bone marrow	Male	2	1	3 (1)	-	1 (1)
	Female	2	-	-	1 (1)	1 (1)
Kidneys	Male	3	2 (2)	-	-	-
	Female	1	1 (1)	-	-	-
Liver	Male	1	-	3 (1)	1 (1)	
	Female	-	2	2 (1)	1 (1)	-
Lungs*	Male	-	3 (1)	1 (1)	-	-
	Female	1	1 (1)	-	-	-
Lymph nodes	Male	-	3 (2)	2	-	-
	Female	1	1 (1)	-	-	-
Skin*	Male	2 (1)	2	-	-	-
	Female	-	-	-	-	-
Spleen	Male	-	1	1 (1)	-	1 (1)
	Female	1 (1)	-	-	-	-

*Lesions were dominated by mononuclear cell infiltrates without typical granulomatous character.
Numbers give the total numbers of affected animals; numbers in brackets indicate how many of the affected animals had been euthanized due to clinical disease prior to the end of the experiment.

Figures 23-29. Graft versus host disease (GvHD), hu-NSG mouse.

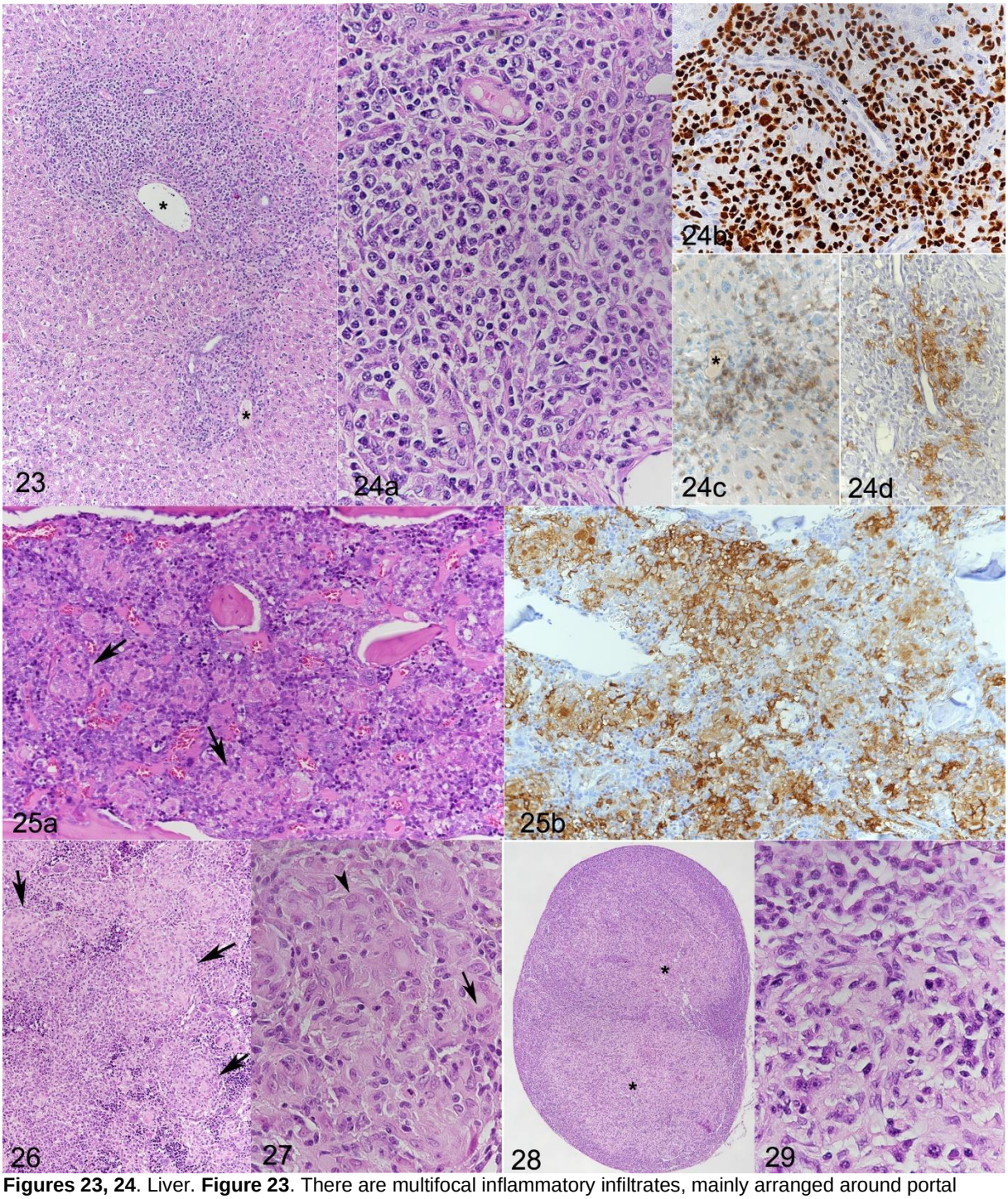

Figures 23, 24. Liver. **Figure 23**. There are multifocal inflammatory infiltrates, mainly arranged around portal areas. Portal vein (*). HE stain. **Figure 24**. **a**. Cells in the focal infiltrates predominantly have the morphology of macrophages and lymphocytes. HE stain. **b**. Almost all cells in the infiltrates are Ku80-positive, confirming their human origin. **c**. A large proportion of cells in the infiltrate are T cells ($CD3^+$). Portal vein (*). **d**. A moderate proportion of cells in the infiltrate are B cells ($CD20^+$). Immunohistochemistry, hemalaun counterstain. **Figure 25**. Bone marrow. **a**. Within the hematopoietic tissue are variably sized aggregates of larger mononuclear cells (arrows). HE stain. **b**. The majority of cells in such focal aggregates are MHC II, suggesting that there are abundant macrophages and activated lymphocytes. Immunohistochemistry, hemalaun counterstain. **Figures 26, 27**. Spleen. **Figure 26**. The red pulp is widely replaced by large granulomatous infiltrates (arrows). **Figure 27**. Closer view of granulomatous infiltrate with epithelioid cells (arrowhead) and multinucleated cells (arrow). HE stains. **Figures 28, 29**. Cervical lymph node. **Figure 28**. The normal architecture is widely replaced by granulomatous infiltrates (*).**Figure 29**. Closer view of granulomatous infiltrate. HE stains.

Correlation between engraftment levels in blood and lymphoid tissues of hu-NSG mice

The FACS analysis performed on the peripheral blood of the hu-NSG mice revealed a large variability in the proportion of human leukocytes (hCD45$^+$), ranging from 0.14% to 66.5% (Fig. 30). As mentioned above, mice with more than 15% hCD45$^+$ cells in the blood were considered as efficiently humanized (Figs. 30a, 31a), and below this threshold as deficiently humanized (Figs. 30b, 31b).

Figures 30, 31. Comparison of efficiently humanized (hu-NSG(e)) and deficiently humanized (hu-NSG(d)) NSG mice.

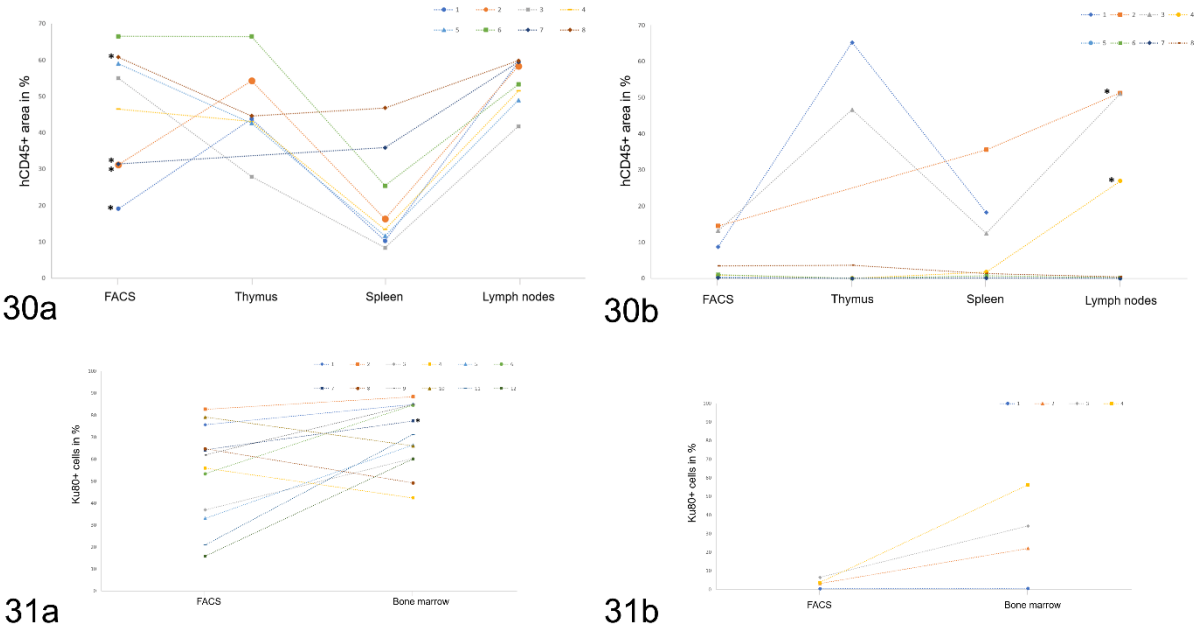

Figure 30. Proportion of human cells in the blood (hCD45$^+$, FACS) and lymphoid organs (hCD45$^+$, immunohistochemistry). **a**. hu-NSG(e) mice. **b**. hu-NSG(d) mice. Each colour represents one individual. Note the large variability among the different individuals but also in the organs of the single individuals. Grouping of the mice followed FACS analysis (cut off 15% hCD45). Lymph node values include the average of all detected lymph nodes in each animal (axillary, cervical and mesenteric). Animals with histological lesions interpreted as GvHD are marked with an asterisk. Only organs without lesions were evaluated. **Figure 31**. Proportion of human cells in the blood (hCD45$^+$, FACS) and bone marrow (Ku80$^+$, immunohistochemistry). **a**. hu-NSG(e) mice. **b**. hu-NSG(d) mice. Each dot represents one individual. Note the large variability among the different individuals but also in the organs of the single individuals, especially in the group of hu-NSG(d) mice. Animals with histological lesions interpreted as GvHD are marked with an asterisk.

Immunohistochemistry against hCD45$^+$ was performed on the lymphoid organs of a proportion of efficiently and deficiently humanized mice (each n = 8) to explore correlation with the FACS data. As expected, this grouping of mice matched to some extent with the degree of repopulation of the hemolymphatic organs, as overall the percentage of human cells was significantly higher in lymph nodes, thymus and bone marrow of the efficiently humanized mice (Table 3). Interestingly, there was no substantial difference in the spleen. This may be due to the overall low relative extent of repopulation of this organ, which still contains a significant proportion of murine hematopoietic cells; even in efficiently humanized mice, the mean percentage area covered by human leukocytes (hCD45$^+$) was 21.0%, whereas it was 46.1% and 54.1% in thymus and lymph nodes respectively (Table 3).

However, looking at repopulation levels in the different organs of individual animals it became obvious that there is substantial variation. Also, a mouse classified as deficiently humanized can have a proportion of human cells in the bone marrow (i.e. the tissue that can be expected to be most relevant for the production of cells that

later appear in the blood stream) that is as high as that seen in efficiently humanized mice (Fig. 8b, d).
The FACS results of animals with histological changes consistent with GvHD (n = 13) were compared with those of mice without such lesions (n = 48). Interestingly, GvHD animals were found to have significantly lower proportions of human leukocytes (Table 5). The human leukocyte population contained significantly lower proportions of lymphocytes and B cells, but significantly higher proportions of T cells and monocytes. There were also significantly more activated T cells, activated T helper cells and activated cytotoxic T cells (Table 5), as confirmed using Spearman's correlation analysis (correlation coefficient of 0.630 for $CD4DR^+$ and of 0.661 for $CD4DR^+$ cells).

Table 5. Cellular composition (proportions) of the peripheral blood in animals with histological evidence of graft versus host disease (GVHD) compared to animals without.

Cell type	Control group		Histological GVHD		P-value and tendency (GVHD vs non-GVHD)	
	Mean	± SD	Mean	± SD		
Leukocytes[a]	63.1%	13.0	39.0%	21.3	0.002	↓
Lymphocytes[b]	74.9%	12.5	53.0%	21.0	0.003	↓
T cells (CD3+)	26.2%	10.6	35.9%	20.1	0.040	↑
B cells (CD19+)	66.5%	11.5	26.1%	9.8	0.020	↓
Activated T cells (CD3+/HLA-DR+)[c]	5.7%	5.0	20.5%	12.3	0.001	↑
Activated T helper cells (CD4+/HLA-DR+) [c]	3.4%	2.7	14.4%	13.3	0.010	↑
Activated cytotoxic T cells (CD8+/HLA-DR+) [c]	9.6%	9.3	29.6%	19.5	0.003	↑
Monocytes[d]	1.7%	0.6	4.6%	2.8	0.002	↑

Human leukocytes (a) were identified based on the expression of hCD45. The hCD45+ cells were subsequently separated further into lymphocytes (b) based on their size in the forward and sideward scatter, as well as T and B cells based on the expression of CD3 and CD19, respectively. HLA-DR co-expression identified activated T cells, activated T helper and activated T killer cells (c), whereas monocytes (d) were cells negative for all other markers, but HLA-DR positive.
Statistical analysis was done using t test.

Discussion

Data illustrating the spectrum of spontaneous and experimentally induced diseases in humanized mice are very limited, and the situation is similar for the recipient NSG immunodeficient mice. Besides, detailed characterization of the morphological aspects of repopulation at tissue level is highly desirable to allow accurate correlation with the engraftment features obtained via FACS analysis. This study aimed to characterise the morphological phenotype of NSG mice and their humanized counterpart, the $CD34^+$ hu-NSG murine model, and to gather data on the most common background lesions in both types of mice. In addition, a comparative quantitative assessment was undertaken in the attempt to relate levels of human repopulation in the hemolymphatic organs of hu-NSG mice to FACS results obtained from the peripheral blood, as the latter is commonly used as a tool to determine the extent of humanization.

Full histological examination of a cohort of 48 NSG mice aged 3 to 6 months revealed a limited spectrum of background lesions, occurring with low severity. Salient changes were observed in lungs, kidneys, testes and adrenal glands and were all among those commonly encountered also in other strains[13,17,39]. In addition, there was a very low prevalence of incidental inflammatory changes, without evidence of infectious conditions. This can likely be ascribed to housing of the mice under specific pathogen free conditions as in general NSG mice are prone to infections because their immune system is compromised.[16] Since the present study focused on young animals, it cannot provide data on potential spontaneous neoplastic processes that might develop with age.[41] Interestingly though, a lymphoma was found in the thoracic cavity of a 6-month-old non-irradiated female NSG mouse, which could have originated from the thymus or the mediastinal lymph nodes. The tumor was predominantly composed of $CD3^+$, $CD4^+$ T cells and further characterized as a T cell lymphoblastic lymphoma. Hematopoietic neoplasms are reported to occur with low prevalence in NSG mice, in subjects older than 1 year,[16,41] due to the inactivation of IL-2Rγ, which plays an important role in the signalling pathways for B and T cell growth.[25] In the present case, it could be a spontaneous event that might have compensated for IL-2Rγ deficiency, and led to full manifestation of the NOD-scid background phenotype, which has been reported to frequently develop lymphomas.[37] Lymphomas, especially thymic lymphomas might also occur secondarily to irradiation, which is used to deplete mouse hematopoietic cells prior to human cell engraftment, or insertional mutagenesis resulting from gene editing therapeutic products. Hence, it is crucial to report on the occurrence of such tumors in untreated NSG mice at an age when they are used in transplantation experiments, to build up an accurate historical database.

All NSG mice in the present study showed poorly developed lymphoid organs, lacking the typical lymphoid tissue architecture. This has previously been reported as a feature in the lymphoid organs of several immunodeficient murine lines, including NSG mice, whose genetic manipulation leads to severe impairment of immune functions.[7,41,42,44] However, we observed small or moderately sized periarteriolar clusters of $mCD45^+$ cells in the spleen of numerous NSG mice, a feature that has so far not been reported. Cells in these clusters did not express more specific lymphocyte or macrophage markers, so further work is needed to assess their exact nature and whether they represent early lymphoid precursors, dendritic or myeloid subsets. According to the experience of the authors, these aggregates can be a confounding factor in studies employing NSG mice engrafted with human hematopoietic cells or administered cell-based therapy products, which might have morphological features similar to these native cells in HE-stained sections. Another

interesting observation was that, like the bone marrow in scid and other immunodeficient mouse lines, the bone marrow of NSG mice did not show major histological abnormalities in the hematopoietic cell component.[14]

The comprehensive histological screening of hu-NSG mice, i.e. NSG mice engrafted with human $CD34^+$ HSC, revealed a spectrum of spontaneous lesions similar to that observed in naïve NSG mice. However, the mice additionally exhibited changes that can be ascribed to either the preconditioning irradiation or the engraftment of human hematopoietic cells.

Among the lesions potentially related to perinatal total body irradiation, to which the *scid* mutation of NSG mice renders them particularly sensitive,[5] were nephropathy, ovarian atrophy and ocular changes, all three well-known complications of radiation exposure in humans.[3,12] Radiation nephropathy has also been described in different preclinical species including mice.[12] In both humans and laboratory animals it represents a late onset, adverse event following external beam irradiation or radionuclide therapy, characterized by concurrent injury to glomerular and tubular compartments.[12,36] In the present study it was observed with low frequency and severity, which suggests an early stage of the disease in the still young hu-NSG mice. So far, both ovarian atrophy and retinal changes have only been sporadically reported as radiation-induced alterations in animal models, and the present report is the first of such lesions in hu-NSG mice undergoing perinatal preconditioning. Interestingly, both types of changes occurred with high prevalence and severity, indicating a high sensitivity of ovaries and retina of these mice to irradiation. It is known that the germline cells in the ovary are highly susceptible to radiation damage and that accelerated reproductive aging can occur when the follicle pool, which is finite and non-renewable, is damaged due to irradiation.[1] From the present findings it could be speculated that radiation-induced damage of the female germ cells at an early prepubertal stage might cause loss of ovarian reserve, which then manifests as atrophy of the gonads and lack of cyclical changes in uterus and vagina. Interestingly, there were no substantial microscopic changes in the testes of hu-NSG mice, suggesting that the irradiation procedure did not affect the male germline. This difference might be due to different radiation exposure or reduced sensitivity of the male gonadal tissues in the postnatal period, as previously reported.[15] Radiation retinopathy in humans encompasses a number of retinal changes following exposure to radiations from any source, typically external beam radiation exposure in patients affected by nasopharyngeal, sinusal or orbital tumors.[3] In animal models, the occurrence of ocular radiation complications has recently been reported as rare, most frequently affecting the lens as cataracts, which also occurred in this study with low prevalence and low severity.[38] The retinal lesions observed in our mouse cohort suggest a perinatal stop of the retinal development, allowing only the neuroblastic layer and the ganglion cell layer to be identified[51], and, to our knowledge, they have not been previously reported in mice that have undergone total body irradiation. Extensive photoreceptor loss and impaired retinal development in the hu-NSG mice might therefore be linked to radiation exposure in the perinatal period, when cell proliferation is still ongoing in the retina as part of the postnatal development process. Nonetheless, a more thorough investigation of the retinal changes was beyond the scope of the present study, as it would require dedicated long-term studies with multiple endpoints and multiple radiation quantities. Notably though, researchers should be aware of potential impaired vision resulting from the retinal lesions.

The changes that can be ascribed to the engraftment of human hematopoietic cells are represented by granulomatous inflammatory infiltrates of almost exclusively human origin that were found in multiple organs of around 20% of hu-NSG mice. The

absence of microorganisms and foreign material and the dominance of macrophages and $CD4^+$ T cells suggest an underlying human-anti-mouse immunopathological process. Accordingly, these granulomatous processes were interpreted as a manifestation of GvHD, a condition that has been reported in several humanized mouse models;[11,20] some of which are employed to study the pathogenesis of GvHD[43]. Typical GvHD lesions described in both mice and humans include T cell-mediated, lymphocyte-rich portal hepatitis, enteritis and dermatitis, and the latter was also observed in some animals in the present study. However, the predominance of granulomatous lesions in 20% of hu-NSG mice points to a loss of human $CD4^+$ T cell tolerance against the mouse host.[11,45] These $CD4^+$ T cell responses might be favored by the NOD mouse strain background of hu-NSG mice. NOD mice spontaneously develop $CD4^+$ T cell mediated autoimmunity in various organs, starting with β-cell destruction in pancreatic islets, leading to diabetes.[50] GvHD has been reported as a major cause of morbidity also in other studies employing humanized mice, however the prevalence of GvHD appears much lower (7% of the reconstituted hu-NSG animals) in the present cohort than in other models.[20,26]. Since the affected mice do not reach the experimental end-point they are often excluded from the analysis and the frequency of the respective pathological changes, whose underlying cause is ascribed to GvHD, is rarely reported.[3] In the present study, GvHD was only observed in one out of thirteen mice that did not show weight reduction or clinical signs, but still exhibited granulomatous lesions, with more males found to be affected (21%) than females (11%). These data indicate that monitoring of weight loss and clinical signs can identify the majority of mice with GvHD. Still, some mice with only few and mild lesions that can only be detected by a histological examination may not be identified and show an aberrant immunological response of the engrafted human cells in different types of experiments. It is important to highlight though that the prevalence and features of GvHD reported here might solely apply to the model employed in our study, as there is growing evidence that the incidence and severity of GvHD varies extensively across experiments depending on the source, number and manipulation of human donor cells employed and the features of the recipient host system (e.g. strain susceptibility, environmental features and preconditioning protocols involving irradiation or chemotherapy).[19,32]

In the present study, the *in situ* detection of human and murine cells in the hemolymphatic tissues provided information on the extent and distribution of homing of graft and host leukocytes after humanization with $CD34^+$ HSC. We observed that the mouse component ($mCD45^+$ cells) generally decreased with humanization of the animal, even though the difference was not statistically significant. This phenomenon cannot be explained without further studies employing larger numbers of animals. It could simply be a consequence of irradiation; alternatively, it is possible that the introduction of human cells leads to a reduced proliferation of the murine leukocytes. Both FACS data and the image analysis of tissue sections of hemolymphatic organs suggested that the extent of $hCD45^+$ repopulation was highly variable among the engrafted animals. The reason for this is not clear, but pre-treatment, injection route and source of HSCs will inevitably have an impact on the inter- and intra-experimental variability of engraftment. This make comparisons across different models difficult, even when experimental conditions vary only slightly. Human cells showed a variable distribution in the different organs. In the spleen, $hCD45^+$ cells formed aggregates reminiscent of the white pulp of immunocompetent mice, despite the absence of discernible PALS and lymphoid follicle organisation. The thymus of hu-NSG mice was variably repopulated by human T cells, providing further evidence of some functional homing of the lymphocytes; however, the typical architecture was

not observed. In the lymph nodes, however, there was no evidence of a cell type specific arrangement. It has previously been suggested that the genetic background of the mice is responsible for the lack of the typical architecture in the lymphoid organs, as cytokines like lymphotoxin (LT) are essential for their appropriate development.[29] The architecture is crucial for the proper functionality of the immune system,[35] and it has been suggested that the poorly organized lymphoid organs are a limiting factor in the humoral immune response of humanized mice.[53] Repopulation of the bone marrow seems to be less complicated; in GvHD lesion-free bone marrows all cell types appeared to home effectively.

The present study also investigated whether there is any correlation between the pattern and extent of reconstitution in the lymphoid organs by human leukocytes and the results of the FACS analysis on the peripheral blood. The FACS analysis revealed a high variability in reconstitution between the different animals, at the same time the actual distribution of $hCD45^+$ in the lymphoid organs of an individual can be quite variable. Upon pairing the obtained FACS data of the reconstitution 3 to 6 months after human HSC injection with the morphological analysis of the lymphoid organs it becomes evident that a high reconstitution does not necessarily go in hand with a high repopulation at the tissue level. In the efficiently humanized mice there was no significant correlation between the level of circulating $hCD45^+$ cells and $hCD45^+$ cells in the organs, whereas a significant correlation was seen in the deficiently humanized animals. This significance may be due to the low $hCD45^+$ cell levels in all the compartments and thus a lower variability.

In the animals affected by GvHD the proportion of human leukocytes and lymphocytes in the blood were significantly reduced compared to mice that did not exhibit evidence of GvHD. This might result from migration of human leukocytes from the blood stream to the sites of injury, similarly to what occurs in infections and sepsis,[47] and by compromised hematopoietic function due to GvHD lesions in the bone marrow, as it was visible in the histological evaluation of some of the animals. However, compared to the cohort not affected by GvHD, the proportion of T cells in the blood was significantly increased, as well as the numbers of activated T cells, activated T helper cells and activated cytotoxic T cells. The increased numbers of T cells fit with the central role of effector graft donor T cells in driving GvHD development.[10,32] Moreover, the granulomatous lesions in the bone marrow of affected animals were dominated by MHC II-positive cells, and also activated T cells are known to express this surface antigen.[28] This hypothesis is supported by a study that shows an increase in the proportion and extent of fluctuation of $CD3^+CD4^+CD8\beta^+$ T cells.[10]

Identification of an increase in T cells, primarily activated helper T cells in the FACS data might help to spot individual mice affected by subclinical GVHD, which could then be confirmed via the histological examination of typically affected organs such as the bone marrow, liver and kidneys.

Acknowledgements
The authors wish to thank the technical staff of the Histology Laboratory, Laboratory for Animal Model Pathology, Institute of Veterinary Pathology, Vetsuisse Faculty, University of Zurich, for excellent technical support.
CM is supported by Cancer Research Switzerland (KFS-4091-02-2017), KFSP-Precision^{MS} of the University of Zurich, the Vontobel Foundation, the Baugarten Foundation, the Sobek Foundation, the Swiss Vaccine Research Institute, Roche, ReiThera and the Swiss National Science Foundation (310030B_182827 and CRSII5_180323).

References

1 Adriaens I, Smitz J, Jacquet P. The current knowledge on radiosensitivity of ovarian follicle development stages. *Hum Reprod Update*. 2009;3;359–377.

2 Antsiferova O, Müller A, Rämer PC, et al. Adoptive transfer of EBV specific CD8+ T cell clones can transiently control EBV infection in humanized mice. *PLoS Pathog*. 2014;8;e1004333.

3 Bawankar P, Barman M, Bhattacharjee H, Soibam R, Paulbuddhe V. Radiation retinopathy after external beam irradiation for nasopharyngeal carcinoma: A case report and review of the literature. *Practical Radiation Oncology*. 2018;6;366–368.

4 Borges HL, Chao C, Xu Y, Linden R, Wang JYJ. Radiation-induced apoptosis in developing mouse retina exhibits dose-dependent requirement for ATM phosphorylation of p53. *Cell Death and Differentiation*. 2004;5;494.

5 Bosma MJ, Carroll AM. The SCID mouse mutant: definition, characterization, and potential uses. *Annu Rev Immunol*. 1991;323–350.

6 Braga-Tanaka I, Tanaka S, Kohda A, et al. Experimental studies on the biological effects of chronic low dose-rate radiation exposure in mice: overview of the studies at the Institute for Environmental Sciences. *Int J Radiat Biol*. 2018;5;423–433.

7 Brehm MA, Cuthbert A, Yang C, et al. Parameters for establishing humanized mouse models to study human immunity: analysis of human hematopoietic stem cell engraftment in three immunodeficient strains of mice bearing the IL2rgamma(null) mutation. *Clin Immunol*. 2010;1;84–98.

8 Brehm MA, Shultz LD, Luban J, Greiner DL. Overcoming current limitations in humanized mouse research. *J Infect Dis*. 2013;S125-30.

9 Brehm MA, Wiles MV, Greiner DL, Shultz LD. Generation of improved humanized mouse models for human infectious diseases. *J Immunol Methods*. 2014;3–17.

10 Brinkman RR, Gasparetto M, Lee S-JJ, et al. High-content flow cytometry and temporal data analysis for defining a cellular signature of graft-versus-host disease. *Biol Blood Marrow Transplant*. 2007;6;691–700.

11 Chandra S, Cristofori P, Fonck C, O'Neill CA. Ex Vivo Gene Therapy: Graft-versus-host Disease (GVHD) in NSG™ (NOD.Cg-Prkdcscid Il2rgtm1Wjl/SzJ) Mice Transplanted with CD34+ Human Hematopoietic Stem Cells. *Toxicol Pathol*. 2019;192623319844484.

12 Cohen EP, Robbins MEC. Radiation nephropathy. *Semin Nephrol*. 2003;5;486–499.

13 Creasy D, Bube A, Rijk E de, et al. Proliferative and nonproliferative lesions of the rat and mouse male reproductive system. *Toxicol Pathol*. 2012;6 Suppl;40S-121S.

14 Custer RP, Bosma GC, Bosma MJ. Severe combined immunodeficiency (SCID) in the mouse. Pathology, reconstitution, neoplasms. *Am J Pathol*. 1985;3;464–477.

15 Forand A, Messiaen S, Habert R, Bernardino-Sgherri J. Exposure of the mouse perinatal testis to radiation leads to hypospermia at sexual maturity. *Reproduction*. 2009;3;487–495.

16 Foreman O, Kavirayani AM, Griffey SM, Reader R, Shultz LD. Opportunistic bacterial infections in breeding colonies of the NSG mouse strain. *Vet Pathol*. 2011;2;495–499.

17 Frazier KS, Seely JC, Hard GC, et al. Proliferative and nonproliferative lesions of the rat and mouse urinary system. *Toxicol Pathol*. 2012;4 Suppl;14S-86S.
18 Gille C, Orlikowsky TW, Spring B, et al. Monocytes derived from humanized neonatal NOD/SCID/IL2Rγ(null) mice are phenotypically immature and exhibit functional impairments. *Hum Immunol*. 2012;4;346–354.
19 Gorin N-C, Piantadosi S, Stull M, Bonte H, Wingard JR, Civin C. Increased risk of lethal graft-versus-host disease-like syndrome after transplantation into NOD/SCID mice of human mobilized peripheral blood stem cells, as compared to bone marrow or cord blood. *J Hematother Stem Cell Res*. 2002;2;277–292.
20 Greenblatt MB, Vrbanac V, Vbranac V, et al. Graft versus host disease in the bone marrow, liver and thymus humanized mouse model. *PLoS ONE*. 2012;9;e44664.
21 Greiner DL, Hesselton RA, Shultz LD. SCID Mouse Models of Human Stem Cell Engraftment. *STEM CELLS*. 1998;3;166–177.
22 Ishikawa F, Yasukawa M, Lyons B, et al. Development of functional human blood and immune systems in NOD/SCID/IL2 receptor γ chainnull mice. *Blood*. 2005;5;1565–1573.
23 Ito M, Hiramatsu H, Kobayashi K, et al. NOD/SCID/gamma©(null) mouse: an excellent recipient mouse model for engraftment of human cells. *Blood*. 2002;9;3175–3182.
24 Ito M, Kobayashi K, Nakahata T. NOD/Shi-scid IL2rgamma(null) (NOG) mice more appropriate for humanized mouse models. *Curr Top Microbiol Immunol*. 2008;53–76.
25 Ito R, Takahashi T, Katano I, Ito M. Current advances in humanized mouse models. *Cell Mol Immunol*. 2012;3;208–214.
26 King MA, Covassin L, Brehm MA, et al. Human peripheral blood leucocyte non-obese diabetic-severe combined immunodeficiency interleukin-2 receptor gamma chain gene mouse model of xenogeneic graft-versus-host-like disease and the role of host major histocompatibility complex. *Clin Exp Immunol*. 2009;1;104–118.
27 Koboziev I, Jones-Hall Y, Valentine JF, Webb CR, Furr KL, Grisham MB. Use of Humanized Mice to Study the Pathogenesis of Autoimmune and Inflammatory Diseases. *Inflamm Bowel Dis*. 2015;7;1652–1673.
28 Lal G, Shaila MS, Nayak R. Activated mouse T-cells synthesize MHC class II, process, and present morbillivirus nucleocapsid protein to primed T-cells. *Cell Immunol*. 2005;2;133–145.
29 Lan P, Tonomura N, Shimizu A, Wang S, Yang Y-G. Reconstitution of a functional human immune system in immunodeficient mice through combined human fetal thymus/liver and CD34+ cell transplantation. *Blood*. 2006;2;487–492.
30 Lang J, Kelly M, Freed BM, et al. Studies of lymphocyte reconstitution in a humanized mouse model reveal a requirement of T cells for human B cell maturation. *J Immunol*. 2013;5;2090–2101.
31 Lysenko V, McHugh D, Behrmann L, et al. Humanized mouse models for hematopoiesis and infectious diseases. *Swiss Med Wkly*. 2017;w14516.
32 MacDonald KPA, Hill GR, Blazar BR. Chronic graft-versus-host disease: biological insights from preclinical and clinical studies. *Blood*. 2017;1;13–21.
33 Mähler Convenor M, Berard M, Feinstein R, et al. FELASA recommendations for the health monitoring of mouse, rat, hamster, guinea pig and rabbit colonies in breeding and experimental units. *Lab Anim*. 2014;3;178–192.

34 Morse HC, Anver MR, Fredrickson TN, et al. Bethesda proposals for classification of lymphoid neoplasms in mice. *Blood*. 2002;1;246–258.
35 Pearson T, Shultz LD, Miller D, et al. Non-obese diabetic-recombination activating gene-1 (NOD-Rag1 null) interleukin (IL)-2 receptor common gamma chain (IL2r gamma null) null mice: a radioresistant model for human lymphohematopoietic engraftment. *Clin Exp Immunol*. 2008;2;270–284.
36 Pellegrini G, Siwowska K, Haller S, et al. A Short-Term Biological Indicator for Long-Term Kidney Damage after Radionuclide Therapy in Mice. *Pharmaceuticals (Basel)*. 2017;2.
37 Prochazka M, Gaskins HR, Shultz LD, Leiter EH. The nonobese diabetic scid mouse: model for spontaneous thymomagenesis associated with immunodeficiency. *Proc Natl Acad Sci U S A*. 1992;8;3290–3294.
38 Ramos MS, Echegaray JJ, Kuhn-Asif Dacvo S, et al. Animal models of radiation retinopathy - From teletherapy to brachytherapy. *Exp Eye Res*. 2019.
39 Renne R, Brix A, Harkema J, et al. Proliferative and nonproliferative lesions of the rat and mouse respiratory tract. *Toxicol Pathol*. 2009;7 Suppl;5S-73S.
40 Rongvaux A, Willinger T, Martinek J, et al. Development and function of human innate immune cells in a humanized mouse model. *Nat Biotechnol*. 2014;4;364–372.
41 Santagostino SF, Arbona RJR, Nashat MA, White JR, Monette S. Pathology of Aging in NOD scid gamma Female Mice. *Vet Pathol*. 2017;5;855–869.
42 Seymour R, Sundberg JP, Hogenesch H. Abnormal lymphoid organ development in immunodeficient mutant mice. *Vet Pathol*. 2006;4;401–423.
43 Shultz LD, Brehm MA, Garcia-Martinez JV, Greiner DL. Humanized mice for immune system investigation: progress, promise and challenges. *Nat Rev Immunol*. 2012;11;786–798.
44 Shultz LD, Lyons BL, Burzenski LM, et al. Human Lymphoid and Myeloid Cell Development in NOD/LtSz-scid IL2R null Mice Engrafted with Mobilized Human Hemopoietic Stem Cells. *The Journal of Immunology*. 2005;10;6477–6489.
45 Sonntag K, Eckert F, Welker C, et al. Chronic graft-versus-host-disease in CD34(+)-humanized NSG mice is associated with human susceptibility HLA haplotypes for autoimmune disease. *J Autoimmun*. 2015;55–66.
46 Strowig T, Chijioke O, Carrega P, et al. Human NK cells of mice with reconstituted human immune system components require preactivation to acquire functional competence. *Blood*. 2010;20;4158–4167.
47 Tanaka J, Sato T, Jones RT, Trump BF, Cowley RA. The pathophysiology of septic shock: responses to different doses of live Escherichia coli injection in rats. *Adv Shock Res*. 1983;101–114.
48 Tanaka S, Saito Y, Kunisawa J, et al. Development of mature and functional human myeloid subsets in hematopoietic stem cell-engrafted NOD/SCID/IL2rγKO mice. *J Immunol*. 2012;12;6145–6155.
49 Theocharides APA, Rongvaux A, Fritsch K, Flavell RA, Manz MG. Humanized hemato-lymphoid system mice. *Haematologica*. 2016;1;5–19.
50 Unanue ER. Antigen presentation in the autoimmune diabetes of the NOD mouse. *Annu Rev Immunol*. 2014;579–608.
51 van Cruchten S, Vrolyk V, Perron Lepage M-F, et al. Pre- and Postnatal Development of the Eye: A Species Comparison. *Birth Defects Res*. 2017;19;1540–1567.
52 Vuyyuru R, Patton J, Manser T. Human immune system mice: current potential and limitations for translational research on human antibody responses. *Immunol Res*. 2011;2-3;257–266.

53 Walsh NC, Kenney LL, Jangalwe S, et al. Humanized Mouse Models of Clinical Disease. *Annu Rev Pathol*. 2017;187–215.
54 Yahata T, Ando K, Nakamura Y, et al. Functional Human T Lymphocyte Development from Cord Blood CD34+ Cells in Nonobese Diabetic/Shi-scid, IL-2 Receptor Null Mice. *The Journal of Immunology*. 2002;1;204–209.
55 Zhang B, Duan Z, Zhao Y. Mouse models with human immunity and their application in biomedical research. *J Cell Mol Med*. 2008;6;1043–1058.

Danksagung

In Büchern, Färbungen und Schnitten ich versank
Hiermit zeige ich meinen Dank:
Anja Kipar, meiner Professorin
Zudem auch Institutsdirektorin
Für die Möglichkeit der Dissertation
Zu lernen über Haferzellen, Splendore Hoeppli und Tubulusdegeneration,
Prof. Thorsten Buch für die Co-Korrektur
So folgte ich der richt‘gen Spur,
Giovanni Pellegrini, der mich begleitet
Mein Wissen mir hat stets erweitert,
Prof. Christian Münz und Hana Zdimerova, PhD
Ohne ihre Mäuse geworden wäre es nie,
Dem Labor, die färbten Tag ein Tag aus,
Meinen Mitdoktoranden, denen gilt Applaus,
Meinen Freunden und Mitbewohnern hier und dort
Für jedes Lächeln und jedes Wort,
Meiner Familie und Eltern in der Ferne
Bei kalten Tagen versprühten sie Wärme,
Bedanken möchte ich mich bei meinem Freund
Der mit mir lacht, weint und auch träumt.

Curriculum Vitae

Vorname Name	Sandra Larissa Elena Blümich
Geburtsdatum	04/06/1992
Geburtsort	Berlin
Nationalität	Deutsch
09/1998 – 07/2004	Borsigwalder Grundschule, Berlin, Deutschland
09/2004 – 07/2011	Gabriele-von-Bülow Oberschule, Berlin, Deutschland
08/2008 – 06/2009	Windsor High School, Windsor - CA, USA
28/06/2011	Abitur, Gabriele-von-Bülow Oberschule, Berlin, Deutschland
10/2011 – 04/2017	Veterinärmedizin, Universität Leipzig, Leipzig, Deutschland
09/2013 - 06/2014	Veterinärmedizin, VetAgro Sup Lyon, Lyon, Frankreich
20/04/2017	Abschlussprüfung vet. med., Universität Leipzig, Leipzig, Deutschland
09/2017 – 01/2020	**Anfertigung der Dissertation** unter Leitung von Prof. Dr. med. vet. Anja Kipar am Institut für Veterinärpathologie der Vetsuisse-Fakultät Universität Zürich Direktorin Prof. Dr. med. vet. Anja Kipar
09/2017 - 02/2019	Internship in Veterinärpathologie am Institut für Veterinärpathologie, Vetsuisse-Fakultät, Universität Zürich, Schweiz
Seit 04/2019	Startup Trainee Medical Functions, Roche Pharma AG Grenzach, Deutschland